

Mathematical study of linear morphodynamic acceleration and derivation of the MASSPEED approach

F. Carraro^a, D. Vanzo^b, V. Caleffi^a, A. Valiani^a, A. Siviglia^b

^a*Department of Engineering, University of Ferrara, Italy*

^b*Swiss Federal Institute of Technology, Laboratory of Hydraulics, Hydrology and Glaciology, Zürich, Switzerland*

Abstract

Morphological accelerators, such as the MORFAC (MORphological acceleration FACtor) approach [24], are widely adopted techniques for the acceleration of the bed evolution, which reduces the computational cost of morphodynamic numerical simulations. In this work we apply a non-uniform acceleration to the one-dimensional morphodynamic problem described by the de Saint Venant-Exner model by multiplying all the spatial derivatives by an individual constant (≥ 1) acceleration factor. The final goal is to identify the best combination of the three accelerating factors for which i) the bed responds linearly to hydrodynamic changes; ii) a consistent decrease of the computational cost is obtained. The sought combination is obtained by studying the behaviour of an approximate solution of the three eigenvalues associated with the flux matrix of the accelerated system. This approach allows to derive a new linear morphodynamic acceleration technique, the MASSPEED (MASs equations SPEEDUp) approach, and the *a priori* determination of the highest acceleration allowed for a given simulation. In this new approach both mass conservation equations (water and sediment) are accelerated by the same factor, differently from the MORFAC approach where only the sediment mass equation is modified. The analysis shows that the MASSPEED gives a larger validity range for linear acceleration and requires smaller computational costs than that of the classical MORFAC approach. The MASSPEED approach is implemented within an example code, using an adaptive approach that applies the maximum linear acceleration similarly to the Courant–Friedrichs–Lewy stability condition. Finally, numerical simulations have been performed in order to assess accuracy and efficiency of the new approach. Results obtained in the long-term propagation of a sediment hump demonstrate the advantages of the new approach.

Keywords:

SWE - Exner model, Morphological accelerators, MASSPEED approach, MORFAC approach, long term morphodynamic evolution

1. Introduction

Reducing the computational costs of numerical simulations of the morphological evolution in rivers, estuaries and coastal areas is a critical issue for engineers and geomorphologists [e.g. 4, 25, 26]. Even

though simulation tools of physical systems have greatly benefited from the increasing computational power over the last decades thanks to progress in CPU performances and parallelization technologies, the use of morphodynamic upscaling techniques is still widely popular and becomes essential when long-term evolutions must be predicted [e.g. 4, 25, 26]. Classical approaches for morphodynamic acceleration have been developed primarily for costal and estuarine applications [6, 13, 24]. Among them, the MORFAC (MORphological acceleration FACtor) approach [14, 24] has been introduced in the context of coastal applications, with the purpose of efficiently describing the overall morphodynamic effect of a high number of repeated tides. The MORFAC approach is now standard in state-of-the-art commercially available numerical morphological codes [23]. It is daily employed by engineers for solving practical problems in costal and estuarine environments [25, 4] and increasingly used for the simulation of river morphodynamics [e.g. 9, 20, 21, 22]. The key idea of the MORFAC approach is to accelerate the morphological evolution increasing the time bottom variations by a given constant (> 1) factor, thus accelerating the morphodynamic processes. This is effectively obtained by multiplying the sediment flux in the Exner equation by a constant (> 1) acceleration factor updating the bed and flow within the same time step. According to Ranasinghe et al. [23] this approach can be adopted only if the morphological response to the hydrodynamic forcing is linear during one morphological time step. Therefore, the key issue in the application of such an approach is to find the maximum acceleration factor (critical MORFAC in the literature) that can be applied in the numerical simulation. One of the first attempts to assess the accuracy and stability of the MORFAC approach has been carried out by Roelvink [24], who also performed a comparison among different acceleration techniques. Even though the recent advancements [15, 23] to develop a theoretical background to detect this value are significant, the critical MORFAC is still often set by trial-and-error procedures [e.g. 9, 20, 21, 22].

The main goal of this paper is to develop a robust theoretical background for the development of linear morphodynamic acceleration techniques. This will be obtained by performing a mathematical study to quantitatively identifying the limit of application for given hydraulic and sediment-transport conditions, thereby overcoming the limits of a trial and error approach. In this work we focus on the one-dimensional morphodynamic problem described by the de Saint Venant-Exner (dSVE) system of equations. The proposed mathematical framework for studying linear morphodynamic accelerations is developed by considering a non-uniformly accelerated dSVE model, i.e. each of the three governing equations (water and sediment continuity, and conservation of momentum) is accelerated by constant acceleration factors (> 1), namely M_{cw} , M_{cs} and M_q . The final goal is to identify the most convenient combination of the three accelerating factors, to be applied within each single time step, for which i) the bed still responds linearly to hydrodynamic changes; and ii) a consistent decrease of the computational time is obtained. The analysis is carried out by studying an approximate solution for the eigenvalues of the flux matrix associated with the accelerated system, taking advantage of the typically small value attained by the ratio between the sediment and the water discharge. This analysis is an extension of that performed by Lyn [17] for the standard de

Saint Venant-Exner (non-accelerated) system. Our aim is that, from the standard MORFAC approach obtained by setting $M_{cw} = M_q = 1, M_{cs} > 1$, to seek the optimal combinations of these. The analysis of the eigenvalues of the non-uniformly accelerated system of the dSVE allows also derivation of a new linear morphodynamic acceleration technique, which has been dubbed MASSPEED (MASs equations SPEEDup). This is obtained by setting $M_{cw} = M_{cs} > 1, M_q = 1$ and is characterized by a larger validity range for linear acceleration and higher computational speed-up to that of the classical MORFAC approach. Finally, the new MASSPEED approach is implemented using an adaptive approach, similarly to that used for implementing the Courant–Friedrichs–Lewy numerical stability condition. It is then applied to the long-term propagation of a sediment hump with the aim of demonstrating that it is able i) to correctly predict the time evolution with and without friction terms; ii) to decrease considerably the computational costs.

The paper is structured as follows: §2 briefly reviews the governing equations and their main mathematical properties. In §3 we present the new general framework for morphodynamic acceleration and in §4 we derive the MASSPEED approach. In §5 we introduce two numerical strategies to compute the maximum acceleration factors. In §6 we present numerical results for the long term propagation of a sediment hump assessing the advantages of the new approach proposed in this paper. Conclusions are drawn in §7.

2. Analysis of the morphodynamic mathematical model

We consider a one-dimensional morphodynamic model, which describes the flow over an erodible bottom. The bed is assumed to be composed of uniform sediments which are transported by the flow as bedload.

2.1. Governing equations

The governing equations are obtained under shallow water conditions imposing mass conservation for the fluid and solid phases and momentum conservation. In one-dimension they read

$$\begin{cases} \frac{\partial h}{\partial t} + \frac{\partial q}{\partial x} = 0, \\ \frac{\partial q}{\partial t} + \frac{\partial}{\partial x} \left(\frac{1}{2}gh^2 + \frac{q^2}{h} \right) + gh \frac{\partial z}{\partial x} = -gh s_f, \\ \frac{\partial z}{\partial t} + \xi \frac{\partial q_s}{\partial x} = 0, \end{cases} \quad (1)$$

where x is the longitudinal coordinate, t is time, $h(x, t)$ and $z(x, t)$ denote the water depth and the bottom elevation respectively, $q(x, t)$ and $q_s(x, t)$ indicate the liquid and bed-load discharge per unit width, g is the gravitational acceleration, s_f is the friction slope and $\xi = 1/(1 - p)$, where p is the porosity of the riverbed (hereafter we assume $p = 0.4$).

The governing system (1) is composed by three partial differential equations (PDEs) in five unknowns, namely $h(x, t)$, $q(x, t)$, $z(x, t)$, $s_f(x, t)$ and $q_s(x, t)$. Therefore, two extra relations are required to close the

system. The friction term is provided by a classical closure, namely

$$s_f = \frac{q^2}{K_s^2 h^{10/3}}, \quad (2)$$

where K_s is the Strickler coefficient. For the sake of simplicity, the bed-load flux is assumed to be a power function of the velocity [10],

$$q_s = A_g u^m, \quad (3)$$

where A_g and m are two constant parameters. Hereafter we assume $m = 3$.

2.2. Eigenvalues and characteristic curves

The system of governing equations (1) (*original system*) can be cast in quasi-linear form as

$$\frac{\partial \mathbf{W}}{\partial t} + \mathcal{A}(\mathbf{W}) \frac{\partial \mathbf{W}}{\partial x} = \mathbf{S}(\mathbf{W}), \quad (4)$$

where \mathbf{W} is the vector of the conservative variables, $\mathcal{A}(\mathbf{W})$ is the flux matrix and $\mathbf{S}(\mathbf{W})$ is the vector of the source terms. It follows from Eq. (1) that

$$\mathbf{W} = \begin{bmatrix} h \\ q \\ z \end{bmatrix}, \quad \mathcal{A}(\mathbf{W}) = \begin{bmatrix} 0 & 1 & 0 \\ c^2 - u^2 & 2u & c^2 \\ \xi \frac{\partial q_s}{\partial h} & \xi \frac{\partial q_s}{\partial q} & 0 \end{bmatrix}, \quad \mathbf{S}(\mathbf{W}) = \begin{bmatrix} 0 \\ -c^2 s_f \\ 0 \end{bmatrix}, \quad (5)$$

where $u = q/h$ is the depth averaged velocity and $c = \sqrt{gh}$ is the propagation celerity of gravitational waves. Using Eq. (3), the two terms on the last row of matrix $\mathcal{A}(\mathbf{W})$ can be written as

$$\psi = \xi \frac{\partial q_s}{\partial q} \quad \text{and} \quad \xi \frac{\partial q_s}{\partial h} = -u\psi \quad \text{with} \quad \psi = 3\xi \left(\frac{q_s}{q} \right) = 3\xi (A_g g \text{Fr}^2), \quad (6)$$

where ψ is the transport parameter, depending on the ratio between the flux of the sediments and the water discharge, while $\text{Fr} = u/c$ is the Froude number. The parameter ψ is usually small ($\psi \ll 1$), at least in the common range of river and coastal typical sediment transport rates. Given these definitions, the flux matrix $\mathcal{A}(\mathbf{W})$ can be rewritten as

$$\mathcal{A}(\mathbf{W}) = \begin{bmatrix} 0 & 1 & 0 \\ u^2 \left(\frac{1}{\text{Fr}^2} - 1 \right) & 2u & \frac{u^2}{\text{Fr}^2} \\ -u\psi & \psi & 0 \end{bmatrix}. \quad (7)$$

The characteristic polynomial and the eigenvalues of (7) are obtained by setting $|\mathcal{A} - \lambda \mathbf{I}| = 0$, where \mathbf{I} is the 3×3 -identity matrix; the characteristic polynomial reads

$$\lambda^3 - 2u\lambda^2 + (\text{Fr}^2 - \psi - 1) \frac{u^2}{\text{Fr}^2} \lambda + \frac{u^3}{\text{Fr}^2} \psi = 0. \quad (8)$$

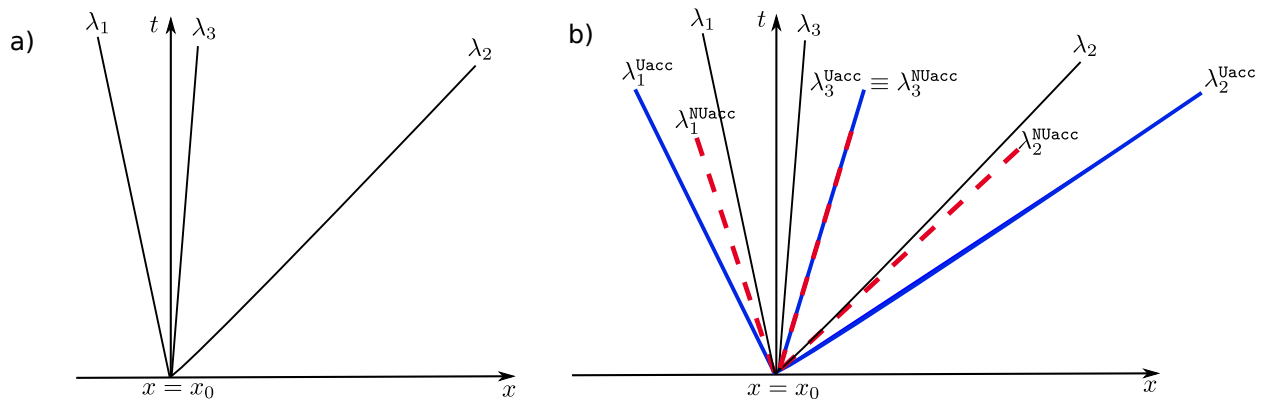


Figure 1: Sketch of (linearized) characteristic curves in the phase space. In panel a) the typical situation for subcritical conditions ($u > 0$) is given. In panel b) the original system (black thin lines) the uniformly accelerated system (Uacc) (blue thick lines) and the non-uniformly accelerated system (NUacc) (red dashed lines) are sketched. The definitions of uniformly and non-uniformly accelerated systems are given in the text.

If a power law formula for the solid transport is used, as that adopted in Eq. (3), the three eigenvalues $\lambda_1, \lambda_2, \lambda_3$, the solutions of the cubic polynomial (8), are always real, therefore the governing system is always hyperbolic [5]. For more general sediment transport formulas, where the non dimensional solid discharge is expressed as a function of the dimensionless Shields parameter (e.g., Meyer-Peter and Müller [19]), if the friction term is closed using a Manning approach, the governing system is hyperbolic provided that $\text{Fr} < 6$ [5]. This latter condition is usually satisfied under *natural* conditions.

On the $(x - t)$ plane (phase space) the eigenvalues are celerities associated to characteristic curves along which small disturbances propagate. Herein, the term celerity is applied broadly to mean the velocity of propagation of a disturbance, either on the water surface or on the bed. For very small disturbances the characteristic curves can be approximated by straight lines. The situation for a small disturbance generated at time $t = 0$ in x_0 , in case of subcritical flow ($\text{Fr} < 1$) is given in Figure 1a.

2.3. Weak interaction between hydrodynamics and morphodynamics: the decoupled system

Though the three roots of the characteristic polynomial (8) can be determined exactly, the derivation of an approximate solution, obtained by a perturbative analysis, is useful for interpretation. Typically, the transport parameter ψ may be estimated as small as $O(10^{-3}-10^{-5})$ [e.g. 12, 15, 17, 18] therefore it seems reasonable to expand λ in powers of ψ as follows:

$$\lambda = \lambda^{(0)} + \psi \lambda^{(1)} + \psi^2 \lambda^{(2)}. \quad (9)$$

We then substitute (9) into Eq. (8), equate likewise powers of ψ and look for the approximate solution of the three eigenvalues λ_i ($i = 1, 2, 3$). At the leading order $O(\psi^0)$, a classical result is found: one of the eigenvalues (λ_3) vanishes and the remaining two reduce to those found in the fixed bed case ($\lambda_{H1, H2}$), namely

$$\lambda_{\text{H1,H2}} \equiv \lambda_{1,2}^{(0)} \cong \lambda_{1,2} = [(\mathbf{Fr} \mp 1) + O(\psi)] c . \quad (10)$$

At the next order $O(\psi)$ small ‘‘morphodynamic’’ corrections for the two hydrodynamic eigenvalues, $\lambda_{1,2}$, are found and the third eigenvalue, associated with bed level changes, arises. Writing also the second order term, λ_3 reads as

$$\lambda_3 \equiv \lambda_b = \left[\left(\frac{\mathbf{Fr}}{1 - \mathbf{Fr}^2} \right) \psi - \left[\frac{\mathbf{Fr} (\mathbf{Fr}^2 + 1)}{(1 - \mathbf{Fr}^2)^3} \right] \psi^2 + O(\psi^3) \right] c . \quad (11)$$

Eq. (11) clearly shows that the present perturbative analysis is valid provided that \mathbf{Fr} is small, in fact when $\mathbf{Fr} \rightarrow 1$, λ_3 tends to infinity. Moreover, by comparing Eq. (10) with Eq. (11) it is seen that the relative order of magnitude of the celerities associated with the characteristic curves of the hyperbolic system is rather different [e.g. 7].

The behavior of such curves is well known: far from the critical state (i.e. $\mathbf{Fr} \ll 1$) the celerity of a small amplitude bed wave is considerably smaller than that of small amplitude hydrodynamic waves [18]. Therefore, the bed interacts only weakly with the water surface, thus justifying an approach in which the equations governing hydrodynamics are solved separately from those governing morphodynamics. It follows that, from a mathematical point of view, the problem can be described separately by the Saint-Venant equations for the hydrodynamics and by a simple nonlinear wave equation for morphodynamics,

$$\frac{\partial z}{\partial t} + \lambda_b \frac{\partial z}{\partial x} = 0 . \quad (12)$$

Taking into account Eq. (10) and Eq. (11), neglecting the friction term and writing the mass and momentum balance laws for the fluid phase in terms of characteristic variables u_1 and u_2 [28], the complete system of governing equations, which approximates system (1) when $\psi \ll 1$, can be written in *decoupled form* as

$$\frac{\partial}{\partial t} \begin{bmatrix} u_1 \\ u_2 \\ z \end{bmatrix} + \Lambda \frac{\partial}{\partial x} \begin{bmatrix} u_1 \\ u_2 \\ z \end{bmatrix} = 0 , \quad (13)$$

where

$$\Lambda = \begin{bmatrix} \lambda_{\text{H1}} & 0 & 0 \\ 0 & \lambda_{\text{H2}} & 0 \\ 0 & 0 & \lambda_b \end{bmatrix} = \begin{bmatrix} (\mathbf{Fr} - 1) + O(\psi) & 0 & 0 \\ 0 & (\mathbf{Fr} + 1) + O(\psi) & 0 \\ 0 & 0 & \frac{\mathbf{Fr}}{1 - \mathbf{Fr}^2} \psi + O(\psi^2) \end{bmatrix} c . \quad (14)$$

According to Eqs. (13), in the phase space ($x - t$ plane), small hydrodynamic perturbations propagate along the characteristic curves $\frac{dx}{dt} = \lambda_{\text{H1,H2}}$ while small bed perturbations travels along the curve $\frac{dx}{dt} = \lambda_b$. From Eqs. (13) emerges that, if $\psi \ll 1$, z is a characteristic variable of the morphodynamic problem. In [Appendix A](#) a linearized example is proposed to validate the decoupled form of the dSVE system.

3. A general framework for morphodynamic acceleration

Small hydrodynamic and bed disturbances propagate along the characteristic curves with celerities given by the eigenvalues of the matrix (7). Therefore, linear acceleration of the propagation of small disturbances can be obtained by increasing the slope of such characteristic curves. If we consider the system of governing equations (4) and neglect friction terms ($\mathbf{S} = \mathbf{0}$), acceleration can be obtained by multiplying from the left the *original* flux matrix by the acceleration matrix \mathcal{M} , namely

$$\frac{\partial \mathbf{W}}{\partial t} + \mathcal{M} \mathcal{A} \frac{\partial \mathbf{W}}{\partial x} = 0, \quad \mathcal{M} = \begin{bmatrix} M_{cw} & 0 & 0 \\ 0 & M_q & 0 \\ 0 & 0 & M_{cs} \end{bmatrix}, \quad (15)$$

in which we consider three scalar acceleration coefficients, M_{cw} for the water continuity equation, M_q for the momentum equation, and M_{cs} for the sediment continuity equation.

In this section two configurations of \mathcal{M} are discussed: a simple case of uniform acceleration (Uacc) of the whole system with $M_{cw} = M_q = M_{cs} = M > 1$, and the case of non-uniform acceleration (NUacc) in which each equation is accelerated by a specific, and in general different, factor ($M_{cw} \geq 1, M_q \geq 1, M_{cs} \geq 1$). In particular, for the non-uniformly accelerated system we present an approximate set of eigenvalues and suitable definitions for the numerical speed-up.

3.1. The trivial case of uniform acceleration (Uacc)

In this section, a *uniformly accelerated* system is analyzed from a computational point of view. We set $M_{cw} = M_q = M_{cs} = M > 1$ in (15) and the resulting system of equations reduce to:

$$\frac{\partial \mathbf{W}}{\partial t} + M \mathcal{A} \frac{\partial \mathbf{W}}{\partial x} = 0. \quad (16)$$

Making use of the eigenvalues and eigenvectors properties, it is easy to verify that all the three eigenvalues of \mathcal{A} scale linearly with M . In other words, we have the uniformly accelerated eigenvalues $\lambda_i^{\text{Uacc}} = M \lambda_i$. In this case, hydrodynamic and morphodynamic information are accelerated linearly by the same factor; therefore, the slopes of the three characteristic curves will be larger and all proportional to M . The corresponding situation in the phase space is depicted in Fig. 1b, where characteristic curves related to the uniformly accelerated system are displayed with thick-blue continuous lines.

It is interesting to analyse the consequences of this acceleration when a numerical solution of system (16) is sought and the adopted scheme must satisfy the Courant-Friedrichs-Lewy (CFL) condition. Here we recall only that the CFL condition is necessary to obtain that the numerical solution (using a finite volume or finite difference method) is stable and converge to the exact solution as the grid is refined [28].

If the spatial domain is discretized with a grid having a constant mesh size Δx , the numerical solution of the original system (4) is advanced in time by a time step Δt that must satisfy the following CFL condition:

$$\Delta t \leq \text{CFL} \frac{\Delta x}{\max(\lambda_i)}. \quad (17)$$

where: CFL is the Courant–Friedrichs–Lewy number with specific values depending upon the selected time integration technique; $\max(\lambda_i)$ is the maximum eigenvalue associated to the flux matrix (7). If we consider $u > 0$, $\max(\lambda_i) = \lambda_2$, as in Fig. 1a. For the uniformly accelerated system the maximum time step that can be adopted is

$$\Delta t_{\text{Uacc}} = \text{CFL} \frac{\Delta x}{\lambda_2^{\text{Uacc}}}. \quad (18)$$

Since $\lambda_2^{\text{Uacc}} = M \lambda_2$, Eqs. (17) and (18) imply

$$\Delta t_{\text{Uacc}} = \text{CFL} \frac{\Delta x}{M \lambda_2} \quad \Rightarrow \quad \Delta t_{\text{Uacc}} = \frac{\Delta t}{M}. \quad (19)$$

This means that, if a uniform acceleration M is imposed, time integration of the accelerated system requires a time step which is M -times smaller to that of the original system. Moreover, to take into account the acceleration of the morphological evolution, the time must be scaled in the accelerated framework. In particular, if we consider a given propagation time t_p related to the simulation performed by using the original system, the corresponding propagation time related to the uniformly accelerated system is t_p/M .

Therefore, the propagation time and the time step in the accelerated framework are both scaled by M , so that the numerical solution at a given output time t_p of the original and the uniformly accelerated systems requires the same number of time steps; *consequently no computational gain is obtained by using the Uacc procedure.*

3.2. The case of non-uniform acceleration (NUacc)

Given the conclusion of the previous section, if a computational gain is sought, a non-uniform acceleration must be considered. The final goal is to find an appropriate combination of the three accelerating factors ($M_{\text{cw}} \geq 1, M_{\text{q}} \geq 1, M_{\text{cs}} \geq 1$) with a twofold objective, as follows:

- (i) *obtaining a linear acceleration for morphodynamics.* This can be obtained when the bottom time evolution can be described by the following accelerated wave equation

$$\frac{\partial z}{\partial t} + M_{\text{cs}} \lambda_b \frac{\partial z}{\partial x} = 0. \quad (20)$$

Therefore, we look for the physical and mathematical conditions under which the accelerated system of governing equations can be written in the decoupled form (13). The linear acceleration allows to precisely describe the propagation of the bed level in the accelerated phase space, providing a linear correspondence between the time scales of the non-accelerated and the accelerated morphodynamic process.

- (ii) *increasing the numerical speed-up.* This means that, if the morphodynamic process is accelerated by a constant factor M_{cs} , the corresponding acceleration of the hydrodynamic process should not reduce the numerical speed-up. That is, the largest eigenvalue of the system of the governing equations (λ_2) must be accelerated by a factor smaller than the morphodynamic acceleration factor M_{cs} .

Graphical representation on the phase space of the two conditions i) and ii) is given in Fig. 1b.

3.2.1. Approximate eigenvalues for the NUacc system

We derive an approximate solution of the three eigenvalues of the NUacc system by taking advantage of the typically small magnitude of ψ and adopting a perturbative analysis similar to that carried out in §2.3. This solution is used in §4 to find the conditions under which a particular choice of $[M_{cw}, M_q, M_{cs}]$ can satisfy the requirement i).

The characteristic polynomial associated to system (15) is obtained by imposing $|\mathcal{M}\mathcal{A} - \lambda\mathbf{I}| = 0$; it reads

$$\lambda^3 - 2M_q u \lambda^2 + M_q (\mathbf{Fr}^2 M_{cw} - M_{cs} \psi - M_{cw}) \frac{u^2}{\mathbf{Fr}^2} \lambda + M_{cs} M_{cw} M_q \frac{u^3}{\mathbf{Fr}^2} \psi = 0, \quad (21)$$

compare this with (8).

Assuming expansion (9) for the solution of equation (21) to $O(\psi)$ we obtain

$$\frac{\lambda_{1,2}^{NUacc}}{c} = M_q \left[\mathbf{Fr} \mp \sqrt{\mathbf{Fr}^2 + \frac{M_{cw}}{M_q} (1 - \mathbf{Fr}^2)} \right] + M_{cs} \left[\frac{\sqrt{\frac{M_{cw}}{M_q} \frac{1 - \mathbf{Fr}^2}{\mathbf{Fr}^2} + 1 + \left(1 - \frac{M_{cw}}{M_q}\right)}}{\sqrt{\frac{M_{cw}}{M_q} \frac{1 - \mathbf{Fr}^2}{\mathbf{Fr}^2} + 1 + \left(1 - \frac{M_{cw}}{M_q}\right) + \frac{1}{\mathbf{Fr}^2} \frac{M_{cw}}{M_q}}} \right] \frac{\psi}{2\mathbf{Fr}}. \quad (22)$$

At $O(\psi^2)$, the celerity associated with the bed level changes is given by

$$\frac{\lambda_3^{NUacc}}{c} = M_{cs} \left[\left(\frac{\mathbf{Fr}}{1 - \mathbf{Fr}^2} \right) \psi - \left(\frac{M_{cs} \mathbf{Fr} (\mathbf{Fr}^2 + 1)}{M_{cw} (1 - \mathbf{Fr}^2)^3} \right) \psi^2 \right]. \quad (23)$$

It is clear that, also for the non-uniformly accelerated system, when $\mathbf{Fr} \rightarrow 1$, $\lambda_3^{NUacc} \rightarrow \infty$. Therefore the assumptions on the perturbation expansion are no longer valid [17].

3.2.2. Theoretical and computational speed-up

The goal of this section is to derive a general theoretical definition for the speed-up of the non-uniform acceleration approach. This is the mean which allows us to quantify the computational gain for a given morphological simulation. We demonstrated that a uniform acceleration applied to both hydrodynamic and morphological evolutions does not result in any computational speed-up. Quite contrary, we expect to have a speed-up when the eigenvalue corresponding to the bottom evolution, λ_3^{NUacc} , is accelerated by a factor M_{cs} compared to the corresponding eigenvalue of the original system $\lambda_3^{NUacc} = M_{cs} \lambda_3$ and at the same time the maximum eigenvalue of the hydrodynamic system, λ_2^{NUacc} , results to be accelerated by a factor $< M_{cs}$ as

compared to its homologous in the original system λ_2 . For the sake of generality, we define the averaged theoretical speed-up over a simulation time T_S as the ratio between the instantaneous morphological $R_M(\tau)$ and hydrodynamic $R_H(\tau)$ acceleration,

$$Sp = \frac{1}{T_S} \int_0^{T_S} \frac{R_M(\tau)}{R_H(\tau)} d\tau. \quad (24)$$

If the condition for Eq. (20) is satisfied, i.e. the NUacc system can be written in a decoupled way, the acceleration terms $R_{M,H}(\tau)$ are the ratio between the accelerated and original eigenvalues,

$$R_M(\tau) = \frac{\lambda_3^{NUacc}(\tau)}{\lambda_3(\tau)}, \quad R_H(\tau) = \frac{\lambda_2^{NUacc}(\tau)}{\lambda_2(\tau)}. \quad (25)$$

It is worth noting that, if the acceleration factors $R_{M,H}$ are set constant over the whole simulation time, equation (24) simplifies to $Sp = R_M/R_H$.

In a similar way we can define the computational speed-up as the ratio between the computational time (CPU time) of the reference solution and the accelerated one,

$$Sp^{CPU} = \frac{CPU(Ref.Sol.)}{CPU(Acc.Sol.)}. \quad (26)$$

4. Linear morphodynamic acceleration techniques

In this section we consider the classical MORFAC (MF) and the newly proposed MASSPEED (MS) acceleration techniques. For both methods, the conditions under which a linear acceleration is possible are identified, and the maximum theoretical speed-up is quantified. Moreover, in [Appendix A](#) a simple application is introduced to explain why the expression of the exact acceleration of λ_3^{NUacc} is a necessary condition to correctly reproduce the riverbed profile with both MORFAC and MASSPEED approaches.

4.1. The classical MORFAC approach

The classical MORFAC approach described in Roelvink [24] is obtained when the acceleration coefficients are set to $M_{cs} = MF > 1$, $M_q = M_{cw} = 1$. Substitution of these values into Eqs. (22) and (23) gives

$$\frac{\lambda_{1,2}^{MF}}{c} = [Fr \mp 1] + O(MF \psi), \quad (27)$$

$$\frac{\lambda_3^{MF}}{c} = \left[\frac{Fr}{1 - Fr^2} \right] (MF \psi) - \left[\frac{Fr (Fr^2 + 1)}{(1 - Fr^2)^3} \right] (MF \psi)^2. \quad (28)$$

The accelerated MORFAC system (15) can be written in the decoupled form (13) if $\lambda_3^{MF} \ll \lambda_2^{MF}$. This condition is satisfied provided that

$$MF \left[\frac{Fr}{1 - Fr^2} \right] \psi \ll [Fr + 1]. \quad (29)$$

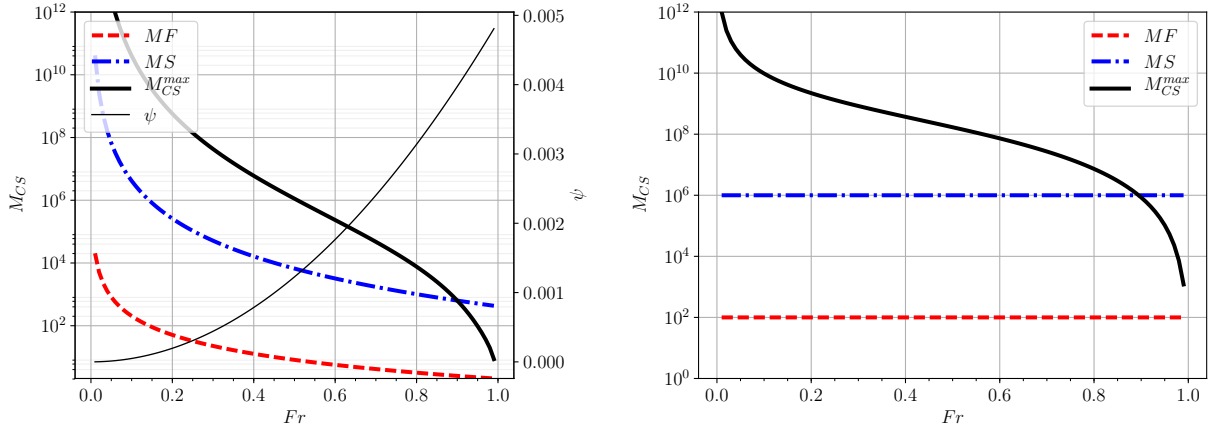


Figure 2: Range of validity for the linear morphodynamic acceleration for MORFAC (red dashed line) and MASSPEED (blue dash-dotted line) techniques. In panel a) the curves are obtained by setting $A_g = 0.0001$, $\epsilon = 0.01$ in relations (30) and (36) and using the definition of ψ in (6). In panel b) the displayed curves are obtained by setting the constant $\psi = 10^{-4}$ in relations (30) and (36).

For Fr numbers typical of environmental flows, i.e. far enough from unity, the term on the left of the inequality (29) is of $O(\text{MF} \psi)$, while the term on the right side is of $O(1)$. Therefore, the resulting range of validity, for which the decoupled approach holds, is

$$\text{MF} \psi = \epsilon \quad (30)$$

where ϵ is a small parameter ($\epsilon \ll 1$). If we set $\epsilon = 0.01$, use the definition of $\psi(\text{Fr})$ and set $A_g = 0.0001 \text{ s}^2/\text{m}$ in (6), and plot expression (30), we obtain the red dashed line in Fig. 2a. This curve identifies the maximum acceleration coefficient MF that preserves a linear morphodynamic acceleration for a given Fr . Therefore the area below the curve represents the whole range of validity of the decoupled approximation. It allows that for small Fr number the acceleration coefficient is very large but rapidly decreases with increasing Fr . It is also worth noting that, for this particular example, the acceleration factor is smaller than unity for $\text{Fr} \gtrsim 0.6$: this means that the decoupled approximation holds only with a deceleration ($\text{MF} < 1$) of the system. Hence, this represents the value beyond which use of the MORFAC approach becomes counterproductive.

It is important to underline that the function $\psi(\text{Fr})$ (thin black line in Fig. 2a) is monotonically increasing but this strongly depends on the chosen transport closure formula (e.g. 6). For the sake of generality we present also the validity range when considering a constant value of ψ (equal to 10^{-4} in Fig. 2b). We, thus, remark that all the subsequent considerations hold both for $\psi(\text{Fr})$ or $\psi = \text{const}$.

If condition (30) holds, in agreement with Li [15], the MORFAC approach does not accelerate hydrodynamics since $\lambda_{1,2}^{\text{MF}} \approx \lambda_{1,2}$ while the bed evolution is linearly accelerated by a factor MF , i.e. $\lambda_3^{\text{MF}} = \text{MF} \lambda_3 + O(\text{MF} \psi)$. The corresponding situation in the phase space is depicted in Fig. 3a.

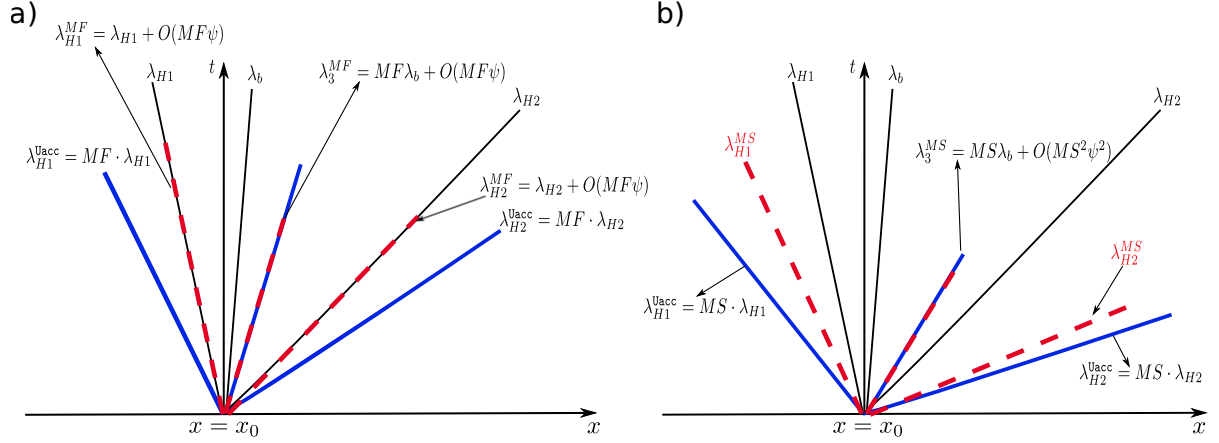


Figure 3: Representation of linearised characteristic curves in the phase space for: original system (black thin lines); uniformly accelerated U_{acc} system (blue thick lines); MORFAC approach (red dashed lines, panel a); MASSPEED approach (red dashed lines, panel b). According to the results given in Fig. 2 MS is always larger than MF.

Substituting (27) and (28) into definition (24), for a given and constant Fr , the expected computational speed-up of the MORFAC method is

$$Sp_{MF} = \frac{\lambda_3^{MF}}{\lambda_3} \cdot \frac{\lambda_2}{\lambda_2^{MF}} \approx MF \cdot 1 = MF. \quad (31)$$

4.2. The MASSPEED approach

The MASSPEED (MS) approach is derived from Eq. (23): if $M_{cw} = M_{cs} = MS$, the eigenvalue associated to the bed evolution λ_3^{MS} scales linearly, up to $O(\psi^2)$, with its analogous in the original system (11), and the scale factor is MS, thus $\lambda_3^{MS} = MS\lambda_3 + O(\psi^2)$. This suggests that, if the sediment continuity equation (Exner equation) is accelerated by a factor M_{cs} , an identical acceleration must be imposed on the water continuity equation. If we set $M_{cw} = M_{cs}$ in Eqs. (23) and (22) and consider the higher order terms, the condition of weak interaction between bed and hydrodynamics, $\lambda_3^{MS} \ll \lambda_2^{MS}$, is satisfied provided that

$$R \left[\frac{Fr}{1 - Fr^2} \right] \psi \ll \left[Fr + \sqrt{Fr^2 + R(1 - Fr^2)} \right] \quad \text{with} \quad R = \frac{M_{cw}}{M_q} = \frac{M_{cs}}{M_q} = \frac{MS}{M_q}. \quad (32)$$

For Fr numbers typical of environmental flows, far enough below unity, the term on the left of the inequality (32) is of order $O(R\psi)$, while the term on the right side is of order $O(R^{1/2})$. Therefore, the analysis of condition (32) implies it to be satisfied if

$$R\psi^2 = \epsilon, \quad \text{with} \quad \epsilon \ll 1. \quad (33)$$

This condition can be transformed on a constraint on MS if a given value is assigned to M_q . At this stage, we found it convenient to set $M_q = 1$. Then, we introduce the MASSPEED approach, defined by the following choice for the acceleration coefficients: $M_{cw} = M_{cs} = MS > 1$, $M_q = 1$. Inserting these values into (22) and (23)

gives

$$\frac{\lambda_{1,2}^{\text{MS}}}{c} = \left[\text{Fr} \mp \sqrt{\text{Fr}^2 + \text{MS} (1 - \text{Fr}^2)} \right] + O(\text{MS} \psi), \quad (34)$$

$$\frac{\lambda_3^{\text{MS}}}{c} = \text{MS} \left[\left(\frac{\text{Fr}}{1 - \text{Fr}^2} \right) \psi - \left(\frac{\text{Fr} (\text{Fr}^2 + 1)}{(1 - \text{Fr}^2)^3} \right) \psi^2 \right]. \quad (35)$$

According to relation (33), the condition for the validity of the decoupled approach assumption is satisfied provided that

$$\text{MS} \psi^2 = \epsilon, \text{ with } \epsilon \ll 1. \quad (36)$$

This range is larger than the analogous range (30), valid for the MORFAC approach. The situation is displayed in Fig. 2, where the blue dash-dotted line is obtained by setting $\epsilon = 0.01$ in both panels. The results is that for all the range of Fr , the MASSPEED allows for larger values of the acceleration coefficient than those given by the MORFAC approach. The areas below these lines represent the range of validity of the decoupled approximation.

Different from the MORFAC approach, the MASSPEED acceleration modifies also the characteristics of hydrodynamics, i.e. $|\lambda_{1,2}^{\text{MS}}| > |\lambda_{1,2}|$ (compare Figures 3a and 3b). In particular, according to (24), $R_{\text{H}} = \lambda_2^{\text{MS}}/\lambda_2 > 1$ hence the theoretical speed-up is bounded as follows:

$$1 < \text{Sp}_{\text{MS}} = \frac{R_{\text{M}}}{R_{\text{H}}} \approx \frac{\text{MS}}{R_{\text{H}}} < \text{MS}. \quad (37)$$

This may wrongly suggest that the MORFAC gives a larger speed-up than MASSPEED, while it is true that the MASSPEED approach allows for much larger values of M_{cs} which compensates by far the reduction of the integration time-step due to the acceleration of the hydrodynamic characteristic λ_2^{MS} .

Since λ_3^{MS} is increased by the rate of R_{M} and λ_2^{MS} by the rate $R_{\text{H}} < R_{\text{M}}$, there is the risk that small morphodynamic disturbances may be accelerated so as to travel faster than the fastest hydrodynamic small disturbances, i.e. $\lambda_3^{\text{MS}} \geq \lambda_2^{\text{MS}}$. Therefore it sounds reasonable to impose a physical limit for the validity of the MASSPEED approach. The physical limit of such an acceleration is given by the fact that the bed wave perturbation associated to λ_3^{MS} should travel at a slower pace than the perturbation of the water surface associated to λ_2^{MS} . Now, if we consider the approximation of λ_2^{MS} , Eq. (34), at the leading order $O(\psi^0)$ and λ_3^{MS} , Eq. (35), at $O(\psi)$, and impose $\lambda_2^{\text{MS}} = \lambda_3^{\text{MS}}$, we obtain the following limit relation

$$\text{MS}^{\text{max}} = - \frac{(\text{Fr}^6 + 2\text{Fr}^4\psi - 3\text{Fr}^4 - 2\text{Fr}^2\psi + 3\text{Fr}^2 - 1)}{\text{Fr}^2\psi^2}, \quad (38)$$

which gives the maximum factor MS^{max} that can be used to avoid this unphysical behaviour. Accelerating the system by a factor $\text{MS} < \text{MS}^{\text{max}}$ avoids the loss of the strict hyperbolicity, which occurs when two eigenvalues coalesce [5, 28]. This particular mathematical condition must be avoided because may give rise to resonance and loss of solution uniqueness. Theoretical issues regarding resonance are found in the classical papers [11, 16] and references therein. In Fig. 2 the condition of the physical validity of (38) is plotted as a function

of the Froude number. It is seen that for $\epsilon = 0.01$ the range of validity for the decoupled solution is contained within the limit of physical validity for all Fr values.

Finally, substitution of Eq. (38) in the definition of the maximum speed-up gives

$$\text{Sp}_{\text{MS}}^{\text{max}} = \text{MS}^{\text{max}} \frac{1 + \frac{1}{\text{Fr}}}{1 + \sqrt{1 + \text{MS}^{\text{max}} \left(\frac{1}{\text{Fr}^2} - 1 \right)}}. \quad (39)$$

If we substitute the definition of ψ and set $A_g = 0.0001$ in (3), and plot relation (39), we obtain the black solid curve in Fig. 4. Moreover, the dashed line is obtained by setting the constant $\psi = 10^{-4}$ in (39). It is observed that the speed-up is of order 10^2 for small Froude numbers and decreases rapidly to unity as $\text{Fr} \rightarrow 1$.

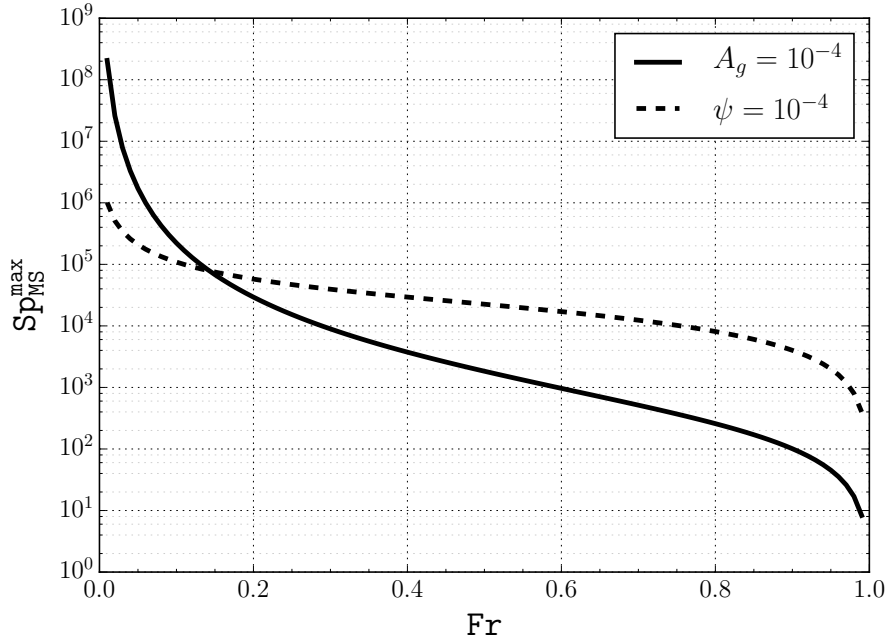


Figure 4: MASSSPEED approach: maximum theoretical speed-up $\text{Sp}_{\text{MS}}^{\text{max}}$ (Eq. 39) obtained from the approximate solution of the eigenvalues. The full line is obtained by using the definition of ψ as in Eq. (6) and setting $A_g = 0.0001$ in the sediment transport closure (3). The dotted line is obtained by setting $\psi = 10^{-4}$.

5. Non-linear numerical strategies to compute the maximum acceleration factors

In the previous section the maximum accelerations allowed with MORFAC and MASSPEED approaches have been introduced thanks to a linear approximation of the system eigenvalues (see §3.2.1). The goal of this section is to defined a more general criterion for the determination of the maximum acceleration factors

by considering the fully nonlinear expression of the three eigenvalues as described in [Appendix B](#). Thus, we propose a further strategy to dynamically recompute the maximum acceleration factors during a numerical simulation. If not differently specified, we consider an acceleration factor $M_{cs} = 10$ and $A_g = 0.005$ in (3).

5.1. Non-linear estimation of the maximum acceleration factors

First we consider the MORFAC approach. The roots associated with the flux matrix $\mathcal{M}\mathcal{A}$ in Eq. (15), can be computed by solving the cubic characteristic polynomial (21) after setting the acceleration factors equal to $M_{cw} = M_q = 1$ and $M_{cs} = MF = 10$, in this example. The MORFAC approach successfully establishes a well defined correspondence between the original and the accelerated model only if morphodynamics evolves linearly in time. More precisely, under the hypothesis of weak interaction between hydrodynamics and morphodynamics, the following relation must hold:

$$R_M = \frac{\lambda_{MF3}(\mathbf{Fr}, MF, \psi)}{\lambda_3(\mathbf{Fr}, \psi)} \approx MF, \quad (40)$$

where λ_3 is the smallest eigenvalue (the morphodynamic eigenvalue) of the original system. Hence, the more R_M deviates from the assigned MF, the weaker the assumption of linear acceleration is. We quantify the maximum acceptable deviation introducing a tolerance band ($\pm To1$), therefore condition (40) can be rewritten as

$$R_M = \frac{\lambda_{MF3}(\mathbf{Fr}, MF, \psi)}{\lambda_3(\mathbf{Fr}, \psi)} = MF (1 \pm To1). \quad (41)$$

Relation (41) is an implicit expression of MF that depends on the water flow (\mathbf{Fr}) and sediment transport (ψ). Hence, for a user-given tolerance ($To1$), the maximum value of MF, which assures that the bed evolves linearly, is numerically computed from Eq. (41). In Figure 5a, the ratios $\frac{\lambda_{MF3}(\mathbf{Fr}, MF, \psi)}{\lambda_3(\mathbf{Fr}, \psi)}$ are displayed by using different style-lines. The ratio λ_{MF3}/λ_3 (red solid line), tends asymptotically to the assigned MF as $\mathbf{Fr} \rightarrow 0$. On the other hand, for increasing values of \mathbf{Fr} the ratio rapidly decays below $MF = 10$. The linear assumption holds as long as the red curve lays inside the grey-shaded areas, corresponding to the right-hand-side of (41): the thinner and the darker the gray stripe is the smaller is the tolerance, $To1 = 5\%$, 1% , 0.1% in this case.

In Fig. 5c the maximum acceleration factor MF, computed with (41), is plotted against \mathbf{Fr} . The three different lines are obtained by considering three different small tolerance values, namely $To1 = 5\%$, 1% , 0.1% . The acceleration coefficient MF shows an inverse exponential dependency on \mathbf{Fr} . This is in agreement with the empirical results obtained by Ranasinghe et al. [23] and Li [15]. It is also seen that the magnitude of the maximum acceleration factor crucially depends on the user-given tolerance.

Finally, for each value MF, the expected numerical speed-up Sp_{MF} (24) is plotted against \mathbf{Fr} in Fig. 5e. As expected, the speed-up is decreasing rapidly for increasing values of \mathbf{Fr} . For example, if we consider $\mathbf{Fr} = 0.1$ and set the tolerance to 1% , the maximum achievable speed-up is about 10 while if we increase the tolerance up to 5% the corresponding speed-up increases up to about 100.

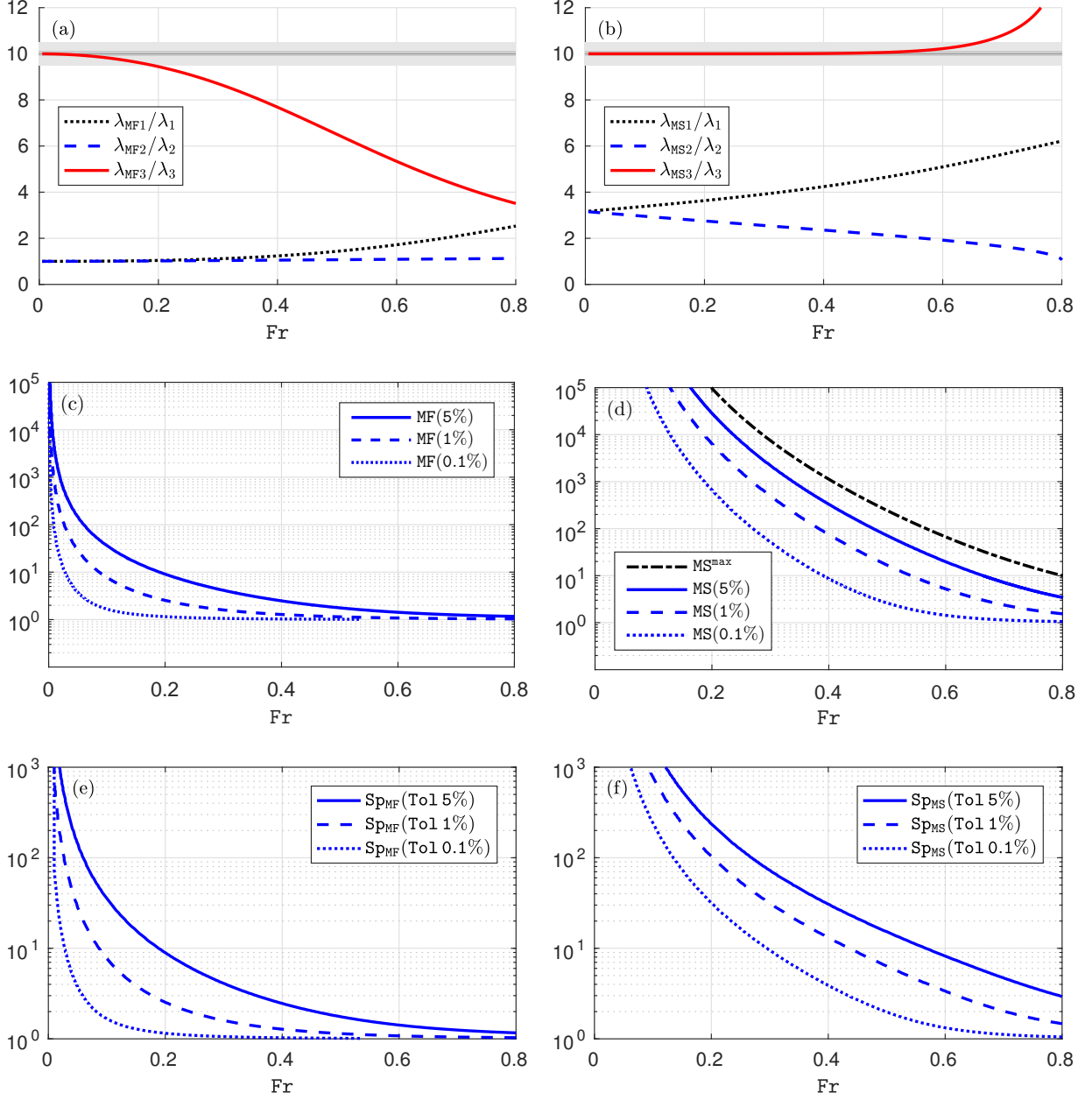


Figure 5: Panel a and b: Ratios of nonlinear eigenvalues $\frac{\lambda_{MF_i}(Fr, MF, \psi)}{\lambda_i(Fr, \psi)}$. The grey-shaded areas represents the tolerance band $To1$ in Eq. (41). Panels c and d: maximum acceleration factor for given values of tolerance. Panels e and f: maximum expected speed-up. In the left and right panels the results for the MORFAC and MASSPEED approaches are collected.

The very same analysis can be extended to the MASSPEED approach, providing $M_q = 1$ and $M_{cw} = M_{cs} = MS$ in the governing system (15). The maximum MASSPEED factor MS for given Fr , ψ and tolerance $To1$ is analogous to (41) and reads

$$R_M = \frac{\lambda_{MS3}(Fr, MS, \psi)}{\lambda_3(Fr, \psi)} = MS (1 \pm To1) . \quad (42)$$

It is interesting to note that, consistently with the results obtained with approximated solutions in §4, the range of Fr numbers for which the ratio $\lambda_{MS3}/\lambda_3 \simeq MS$ (range of linearity), is broader for the MASSPEED when compared with the MORFAC approach. Comparing Fig. 5a and Fig. 5b, the linear range extends up to $Fr \approx 0.6$ (panel b) for the MORFAC, while it reduces to $Fr \approx 0.15$ for the MORFAC (panel a). Within the linear range, the MASSPEED approach shows also higher values of the maximum acceleration (Fig. 5c versus 5d) and larger speed-up (Fig. 5e versus 5f). For example, given a tolerance of 1% and $Fr = 0.4$, the maximum MS corresponds to 75 (Fig. 5d) resulting in a speed-up of about 13 (Fig. 5e) while application of the MORFAC approach does not result in any acceleration.

Finally, concerning the loss of hyperbolicity, we compute the value MS^{\max} by imposing that $\lambda_{MS2} = \lambda_{MS3}$ and making use of the fully nonlinear expression of the eigenvalues. MS^{\max} is plotted against the Fr number in Fig. 5d for a given tolerance of 5% (black dashed line). It is worth noting that the loss of hyperbolicity occurs outside the domain of linear acceleration, i.e. $MS^{\max} > MS(5\%)$.

5.2. Numerical evaluation of the highest acceleration factor: fixed and adaptive approach

Here we propose a numerical strategy similar to the well-known Courant-Friedrichs-Lewy stability condition to maximize the computational speed-up. Note that here we refer only to MASSPEED approach, given that the very same procedure can be implemented for the MORFAC approach.

Let us consider a physical domain of length L discretized with a finite set of points or volumes, regardless if finite difference or finite volume approaches are used. At a given time, within a single numerical time step Δt , local flow (Fr_i) and sediment transport (ψ_i) conditions are assigned and therefore the calculation for each cell i of the nonlinear eigenvalues $\lambda_{MSj,i}$ and $\lambda_{j,i}$ (with $j = 1, 2, 3$) is possible. Then, for a given tolerance value $To1$ (prescribed by the user), application of relation (42) gives the value of the maximum accelerator factor MS_i for each cell i at a given time. Now, two possible approaches are introduced here: fixed and adaptive. In the fixed approach, the maximum acceleration factor MS is computed at the beginning of the simulation as $MS = \min_i [MS_i]$ and kept constant for all time steps of the simulation, until the final time is reached. In the adaptive approach the maximum acceleration factor is a function of time, i.e. $MS_i(\tau)$, and is computed for each time step according to the local flow and sediment transport conditions. Then, for the generic time τ , the adaptive $MS(\tau) = \min_i [MS_i(\tau)]$ is computed solving the following equation for each cell i :

$$\frac{\lambda_{MS3,i}(Fr_i(\tau), \psi_i(\tau), MS_i(\tau))}{\lambda_{3,i}(Fr_i(\tau), \psi_i(\tau))} = (1 \pm To1) \cdot MS_i(\tau) . \quad (43)$$

Eq. (43) is valid for any closure for the solid transport and can be solved via a numeric iterative method (e.g. standard regula falsi (RF) method [29]). Alternatively, to reduce the computational cost due to the iterative procedure, one can obtain $\text{MS}_i(\tau)$ followed for obtaining the curves in Fig. 3.

6. Evolution of a sediment hump: linear and numerical solutions

We assess and compare the accuracy and efficiency of the MORFAC and the new linear morphodynamic accelerator MASSPEED by considering the propagation of a sediment hump. In all cases, the solutions obtained with MORFAC and MASSPEED are compared with that obtained with the original model. First, we solve a linearized problem for which an analytical solution is available. We use this problem as a *proof of concepts* of the theoretical background we developed. Second, we solve numerically the long-term evolution of a sediment hump. The final goal is to assess the advantages of the new MASSPEED approach. Numerical integration is performed by using a classical one-dimensional finite volume scheme. We adopt a path-conservative solver of the DOT [8] type where the use of the analytical formulation of the eigenstructure of the system flux matrix improves the computational efficiency [2, 3].

6.1. Linearized morphodynamic problem: evolution of a small sediment hump

We consider the evolution of a small (infinitesimal) erodible hump due to a nearly uniform water flow in a straight channel. Under these conditions, the problem can be studied within a linear framework, and an analytical solution can be easily derived [e.g. 18]. We consider the original nonlinear system (15) (the friction term is neglected) and perform a linearization by *freezing* the flux matrix (7), or more specifically its entries, considering the following uniform reference state, $\mathbf{W}_L = [h_L, q_L, z_L]^T$. The resulting *linearized system* is

$$\frac{\partial \mathbf{W}}{\partial t} + \mathcal{M} \mathcal{A}_L \frac{\partial \mathbf{W}}{\partial x} = 0, \quad (44)$$

with

$$\mathcal{A}_L = \begin{bmatrix} 0 & 1 & 0 \\ c_L^2 - u_L^2 & 2u_L & c_L^2 \\ -u_L \psi_L & \psi_L & 0 \end{bmatrix} \quad \mathcal{M} = \begin{bmatrix} \text{M}_{\text{cw}} & 0 & 0 \\ 0 & 1 & 0 \\ 0 & 0 & \text{M}_{\text{cs}} \end{bmatrix}. \quad (45)$$

The original system is obtained when $\text{M}_{\text{cw}} = \text{M}_{\text{cs}} = 1$, the MORFAC system for $\text{M}_{\text{cw}} = 1$, $\text{M}_{\text{cs}} = \text{MF}$ and the MASSPEED for $\text{M}_{\text{cw}} = \text{M}_{\text{cs}} = \text{MS}$. Subscript L refers to the reference state and $u_L = q_L/h_L$ and $c_L = \sqrt{g h_L}$ are the reference flow velocity and celerity, respectively. $\psi_L = \psi|_{\mathbf{W}_L} = 3 g \xi A_g \text{Fr}_L^2$ is the reference sediment transport parameter where $\text{Fr}_L = u_L/c_L$ is the reference Froude number and $q_0 = q_L = \sqrt{h_L^3 g \text{Fr}_L^2}$. The initial conditions of the problem are given by $\mathbf{W}_0 = [h_0, q_0, z_0]^T$ with $z_0(x) = z_{\text{max}} \exp(-x^2)$, $z_{\text{max}} = 1.0^{-5}$ m and $h_0(x) = h_L - z_0(x)$. We also assume $\psi_L = 0.01$ and $h_L = 1$ m to which correspond $\text{Fr}_L = 0.33$. The solution of system (44) can be obtained analytically by using characteristic variables [28] as done by Lyn

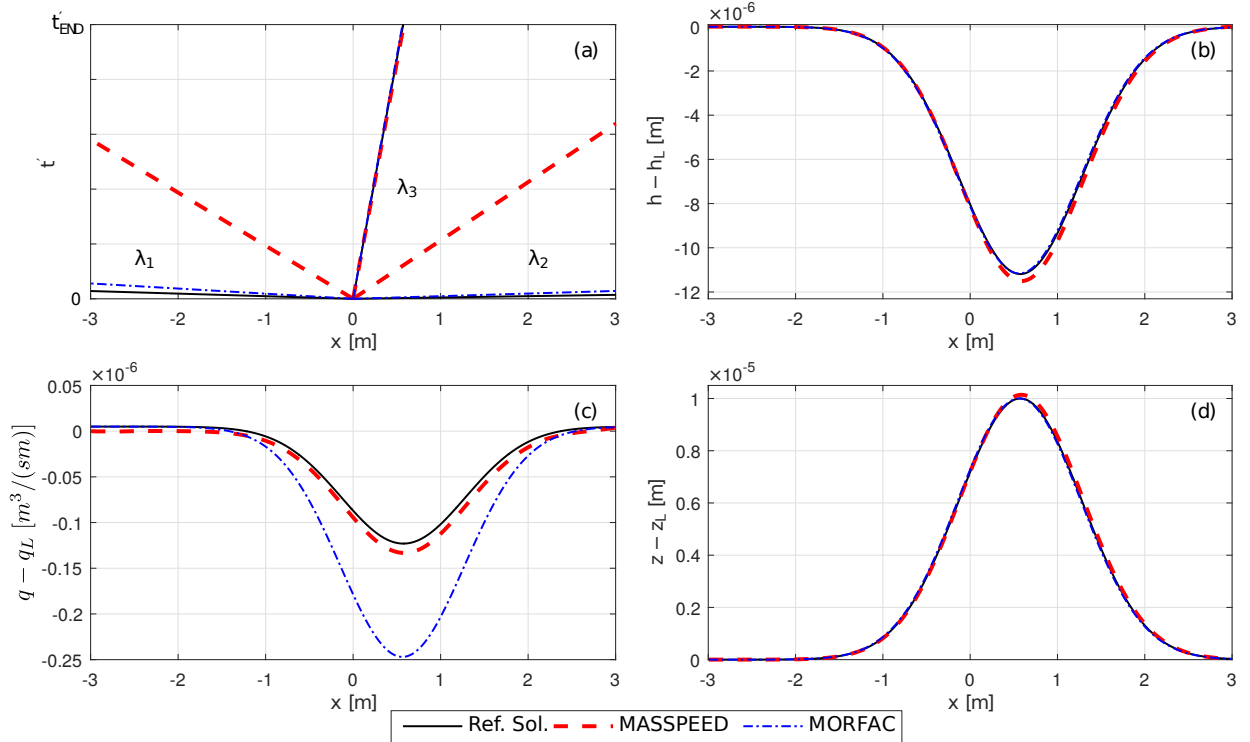


Figure 6: Linearized solution of the propagation of a sediment hump [18] using the linearized MORFAC and MASSPEED approaches: a) comparison between the characteristic lines (the time is properly scaled for the MORFAC and MASSPEED approaches); b) difference between the water depth and the unperturbed water depth; c) difference between the flow discharge and the unperturbed flow discharge; d) bottom elevation. The analytical solution of the linear original system is used as reference.

and Altinakar [18]. More details on how the linear analytical solution is obtained are given in [Appendix A](#). The final time for which the solution is sought is $t_{\text{END}} = 50$ s for the original system. Since the infinitesimal amplitude of the hump, linear conditions hold and therefore the time scales of the accelerated and original system are linked by a linear relation, i.e. the corresponding final time of the simulation for the MORFAC and MASSPEED approaches yields $t_{\text{END},s} = t_{\text{END}}/\text{MF}$ and $t_{\text{END},s} = t_{\text{END}}/\text{MS}$, respectively. Setting a tolerance $\text{To1} = 1.36\%$, the resulting (rounded) maximum acceleration factors, calculated from Eqs. (41) and (42), are $\text{MF} = 2$ and $\text{MS} = 900$. The analytical solutions are displayed in Fig. 6. In Fig. 6a the characteristic lines in the phase space $x - t'$ are given, where t' stands for t the time in the original system, t/MF and t/MS , the times in the MORFAC and MASSPEED systems. Deviations of the water depth, discharge and bed elevation, to their unperturbed initial values h_L , q_L and z_L are given in Fig. 6b, Fig. 6c and Fig. 6d, respectively.

It is seen in the phase space plots, the three eigenvalues with the propagation of bed information, $\lambda_3 \equiv \lambda_3^{\text{MF}} \equiv \lambda_3^{\text{MS}}$, overlap each other (Fig. 6a). As a consequence the celerity of the infinitesimal bed form

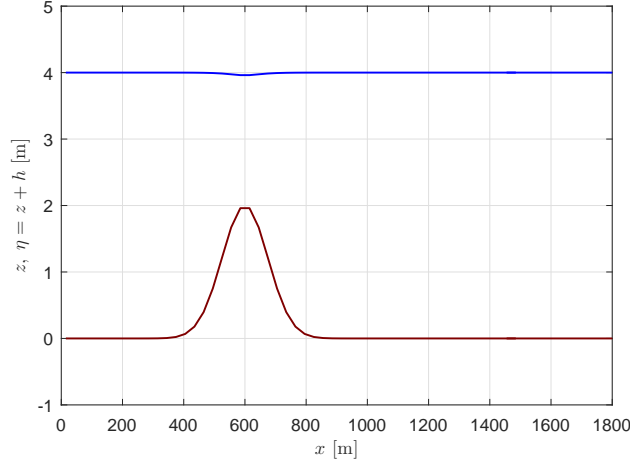


Figure 7: Long term evolution of a bottom hump: initial water surface elevation (blue) and bed elevation (red) profiles.

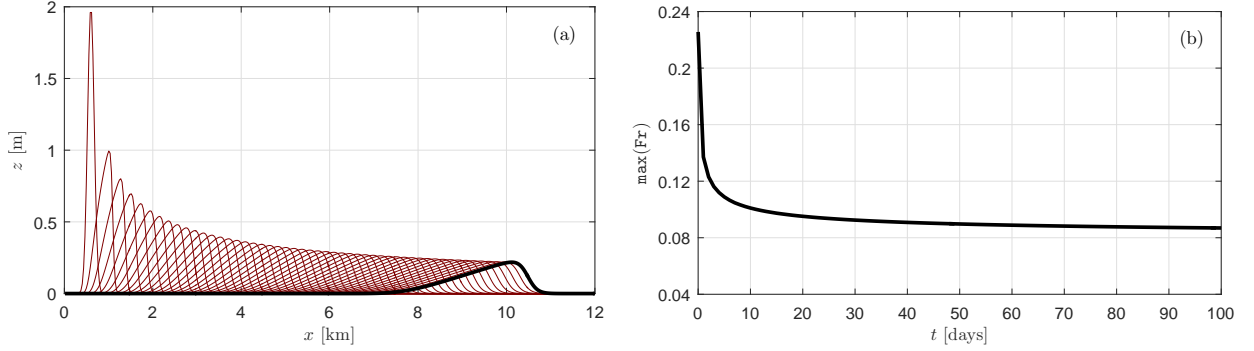


Figure 8: Reference solution for the long term evolution of a bottom hump: a) bottom profiles every two days, in thick line day number 100; b) time evolution of the maximum Fr measured within the numerical domain.

is well predicted by both the MORFAC and MASSPEED approaches (see also Fig. A.13 in Appendix A). It is also seen that the amplitude of water depth (Fig. 6b) and bed elevation (Fig. 6c) are also accurately predicted. A marked difference is found for the water discharge (Fig. 6c) for which the MORFAC approach introduces a larger deviation to that of MASSPEED.

6.2. Long term evolution of a bottom hump: frictionless case

This test case consists of the simulation of the long term evolution of an erodible bottom hump immersed into a quasi-steady, frictionless flow; it is similar to the test proposed by Ranasinghe et al. [23]. The initial bed profile is given by

$$z(x, 0) = z_{\max} \exp \left[-\frac{(x - \mu)^2}{\sigma^2} \right], \quad (46)$$

where $z_{\max} = 2$ m, $\mu = 600$ m and $\sigma = 150$ m. The initial uniform water discharge is $q(x, 0) = q_0 = 2$ m³/(s m) while the initial water depth corresponds to the steady state water profile for the given discharge and

Table 1: Long term evolution of the bottom hump: acceleration parameters (MF, MS and Tol), number of computational time steps, CPU time, numerical (26) and theoretical (24) speed-up, normalized error E_z and final position of the hump crest.

#	Method	Acc. Factors	Time steps	CPU [s]	Sp^{CPU}	Sp	E_z	x(crest) [m]
0	Ref. Sol.		2 050 300	6803	-	-	-	10125
1		$MF_{5.0\%} = 7.1$	291 600	926	7.3	7.1	1.53e-1	10005
2	MORFAC	$MF_{1.0\%} = 2.2$	940 400	3014	2.3	2.2	2.98e-2	10095
3		$MF_{0.1\%} = 1.1$	1 848 700	6013	1.1	1.1	2.81e-3	10125
4		$MS_{5.0\%} = 13\ 049$	16 801	57	119	103	1.19e-2	10125
5	MASSPEED	$MS_{1.0\%} = 2\ 985$	34 802	114	60	50	4.17e-3	10125
6		$MS_{0.1\%} = 304$	109 101	353	19	16	1.06e-3	10125
7		$MS_{5.0\%}$	2 236	9	782	836	3.81e-1	10485
8	A-MASSPEED	$MS_{1.0\%}$	4 700	16	413	404	9.36e-2	10215
9		$MS_{0.1\%}$	14 234	48	141	132	1.19e-2	10125
10		$MS_{0.01\%}$	44 443	150	45	42	1.61e-3	10125

initial bed topography. A constant discharge q_0 is imposed at the upstream boundary while a constant water depth $h_0 = 4$ m is imposed at the downstream boundary. Fig. 7 shows the initial flow and bed configuration. Transmissive downstream boundary conditions are imposed for the bed and A_g is set to 0.005 s²/m in the sediment transport formula (3). The numerical domain ($x \in [0; 12000]$ m) is discretized with 400 cells of constant width (30 m). Finally, t the morphodynamic output time is set equal to 100 days.

Fig. 8a shows the bottom evolution in time, with a temporal breakdown of 2 days, obtained with the original, non-accelerated model. In the first simulated days, the amplitude of the hump decreases rapidly and after about 20 days the bottom assumes a flatter and stable profile. The decrease of the hump amplitude is associated to a corresponding decrease of the maximum Froude number on the computational domain (Fig. 8b).

For this test we performed 10 different runs summarized in Tab. 1. The approach used is specified in column 2, while the acceleration factors and the tolerance used to compute them is specified in the column. Runs 1 to 3 implement the MORFAC approach ($M_{cw} = M_q = 1$, and $M_{cs} = MF$), with tolerance Tol equal to 5%, 1% and 0.1% respectively. Runs 4 to 6 implement the MASSPEED approach ($M_q = 1$, and $M_{cw} = M_{cs} = MS$), with the same tolerances as the previous set. The constant factors MF and MS are computed by using (41) and (42), respectively and considering the highest Froude number of the simulation. In this test the maximum Froude number corresponds to the initial maximum value $Fr \approx 0.23$, as shown

in Fig. 8b. Finally, runs 7 to 10 implement the adaptive version A-MASSPEED, tested with tolerances $\text{To1} = 5; 1; 0.1; 0.01$ [%].

The accuracy of the accelerated solutions with respect to the reference solution is evaluated qualitatively in terms of the final position of the hump crest and, quantitatively, via the normalized root square error E_z , defined as

$$E_z = \frac{\sqrt{\sum (z - z_{\text{ref}})^2}}{\sqrt{\sum z_{\text{ref}}^2}}, \quad (47)$$

where z and z_{ref} are the bottom profiles at the end of the simulation for the given accelerated model (MORFAC or MASSPEED) and the original system. The computational costs and accuracy of the 10 runs are also specified in Tab. 1, while some examples of final bottom profiles are depicted in Fig. 10.

As a first robustness assessment, it is worth noting that the accuracy (E_z and crest position) increases when reducing the tolerance To1 for all the acceleration strategies. Table 1 highlights also the significant differences of computational speed-up between the tested approaches: i.e. MORFAC and A-MASSPEED have speed-up differences of roughly one order or magnitude. Moreover, it is important to underline that the theoretical speed-up Sp is always fairly close to the measured Sp^{CPU} (see §3.2.2). Hence the theoretical formulation can be adopted as a good *a priori* estimation of the effective simulation speed-up.

To better focus on the differences between the investigated strategies, let us discuss Fig. 9, where the numerical speed-up Sp^{CPU} of the 10 accelerated runs are plotted against the normalized errors E_z . It is worth noting that the plot is in log-log scale. Beside the evident increase of the computational speed-up offered by the new proposed approaches with respect to MORFAC, Fig. 9 sheds the light on the accuracy differences of the three methods for a given To1 . In particular, it appears that for the same given To1 , i) MASSPEED is more accurate than MORFAC and ii) the adaptive A-MASSPEED is less accurate than both fixed methods. To justify issue i), please note that for the MORFAC and MASSPEED methods we *fix* the acceleration factors MF and MS (values in Tab. 1) for the entire run based on the maximum expected Froude number and the given tolerance. If the Froude number decreases during the simulation, as in the given test, the error on the linearity assumption (41) also decreases, being a function of Fr (Fig. 5a and b). Nevertheless, the error reduction is faster for the MASSPEED approach, i.e. the ratio of the bottom eigenvalue (red solid line) in Fig. 5b tends to the constant factor MS faster than the corresponding ratio in Fig. 5a. Given this difference in the error reduction rate, the accumulated final error of the MASSPEED method is reduced with respect to MORFAC.

Issue ii) well underlines the main difference between the *fixed* approach (MORFAC and MASSPEED) and the *adaptive* one (A-MASSPEED). This accuracy gap is evident also in Fig. 10, where final bottom profiles are plotted for some selected runs. For given $\text{To1} = 1\%$, MORFAC and MASSPEED profiles are very close to the reference solution, while the A-MASSPEED solution shows an offset of the crest position. As previously discussed, the effective error on the linearity Eq. (41) decreases during the simulation time

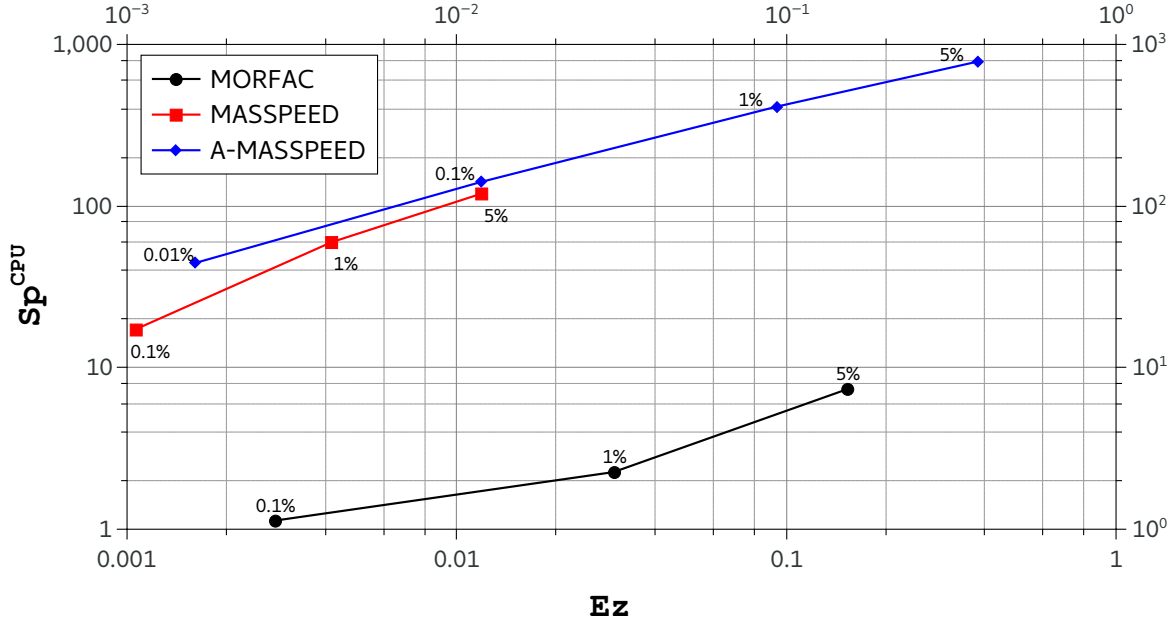


Figure 9: Numerical speed-up Sp^{CPU} against normalized errors E_z for the 10 accelerated runs. Marker labels highlight the user-defined tolerances resumed in Table 1.

when using the *fixed* approaches. On the other hand, with A-MASSPEED, the *adaptive* acceleration factor MS is not bonded by Fr^{max} , but instead recomputed at each time step. This means that the error on the linearity assumption (41) is dynamically forced to be constant and equal to the user-defined $To1$. Such different behavior of the error, decreasing with the fixed strategy but constant with the adaptive one, results in the final greater error of the latter.

Even if, for a given user-defined $To1$, the *adaptive* strategy is less accurate, it is important to highlight that it globally outperforms both the *fixed* methods: as a matter of fact, for any accuracy (error E_z), A-MASSPEED provides the highest numerical speed-up (Fig. 9). Moreover, this method has a further benefit related to the robustness. In fact with the *fixed* approach, we need to know *a priori* the maximum Froude number occurring during the simulation. For very simple applications, as in the test presented here, this prediction is straightforward but in case of more complex hydro-morphological configurations this might not be possible. A "wrong" initial setting of the constant acceleration factors may lead to a final numerical solution that did not satisfy the linearity conditions, hence to a non-linear acceleration of the morphological evolution. In the worst case, a wrong constant factor leads to the loss of hyperbolicity of the accelerated system, hence to a completely failing numerical solution. On the contrary, such troubles are inherently handled by the *adaptive* strategy, where the acceleration factors are dynamically recomputed to keep the acceleration within the linearity threshold.

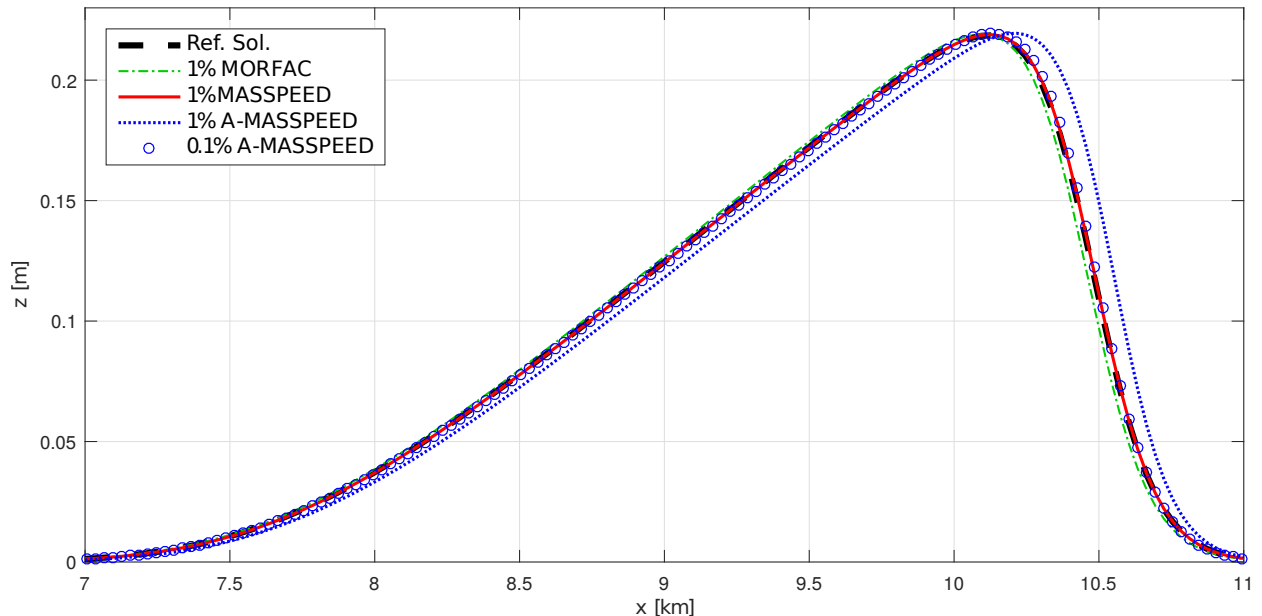


Figure 10: Bottom hump profiles after a 100 days evolution: comparison between reference solution (thick black), MORFAC (run 2), MASSPEED (run 5) and A-MASSPEED (runs 8,9) models.

6.3. Long term evolution of a bottom hump: bottom friction case

The main goal of this test is to verify that the friction term does not alter the main features of the accelerated models. To account also for the bottom friction term into the accelerated framework, system (15) can be rewritten as

$$\frac{\partial \mathbf{W}}{\partial t} + \mathcal{M} \mathcal{A}(\mathbf{W}) \frac{\partial \mathbf{W}}{\partial x} = \mathcal{M} \mathbf{S}(\mathbf{W}), \quad (48)$$

where $\mathbf{S}(\mathbf{W})$ is the vector of the source terms defined in (5) and \mathcal{M} is the acceleration matrix. It is important to note that $\mathcal{M} \mathbf{S}(\mathbf{W}) = [0, -M_q c^2 s_f, 0]^T$ and $M_q = 1$ in both MORFAC and MASSPEED approaches. Therefore, the accelerations of the models do not influence the expression of the friction source term.

From a numerical point of view, the source term is treated by using a classical splitting procedure (e.g. [27]). Without loss of generality, we present the results only for the adaptive A-MASSPEED approach, assuming $To1 = 0.001$.

The test is a modification of that given in the previous section (same boundary conditions), where we add a constant slope $s_0 = 0.1\%$ to the initial bed profile, thus,

$$z(x, 0) = -s_0 x + z_{\max} \exp \left[-\frac{(x - \mu)^2}{\sigma^2} \right]. \quad (49)$$

Assuming a water discharge $q_0 = 2 \text{ m}^3/(\text{s m})$ and constant Strickler roughness $K_s = 19.8 \text{ m}^{1/3} \text{ s}^{-1}$, the resulting normal flow depth is $h_0 = 4 \text{ m}$. Fig. 11a shows the initial water surface and bottom elevation profiles. The simulated time is 50 days.

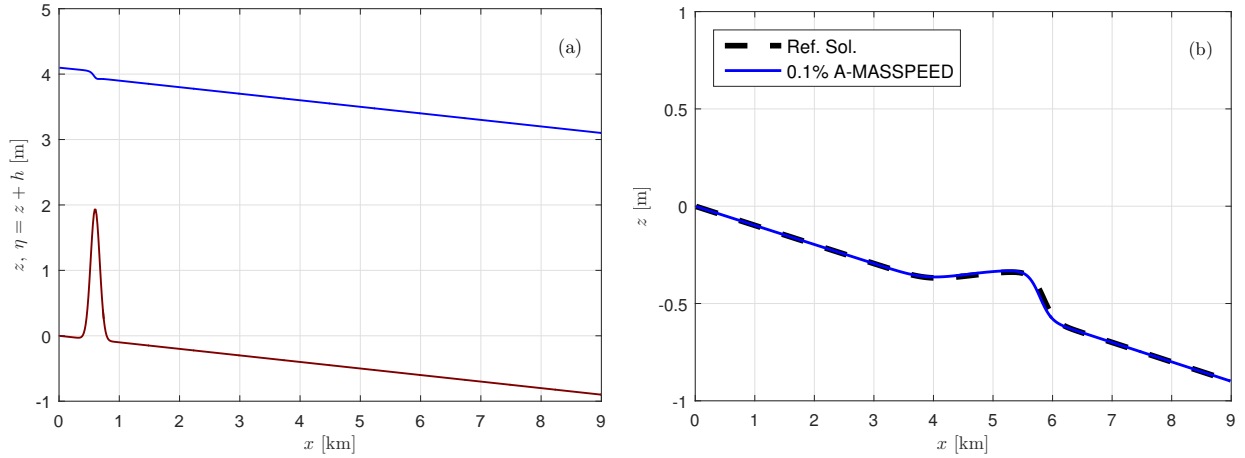


Figure 11: Treatment of the friction source term: (a) initial condition of the Hump test with not negligible friction; (b) results of a 50 days long morphodynamic simulation of the hump evolution.

Fig. 11b shows the comparison between the bottom profile at the end of the simulation, obtained using the A-MASSPEED approach, and the corresponding reference solution. It is seen that the solutions are in good agreement. Moreover, the error E_z computed by using relation (47), is equal to $1.3e-2$, i.e., of the same order of magnitude of the errors obtained by neglecting the friction term (see Tab. 1). Analogous results, here omitted for the sake of brevity, can be obtained by using the MORFAC approach.

7. Conclusions and future trends

In this paper we carried out a mathematical study to identify the conditions under which bed evolution, governed by the one-dimensional dSVE equations, can be linearly accelerated. This was achieved by introducing the concept of non-uniform acceleration, consisting by multiplying the spatial derivatives of each of the three governing equations by a constant acceleration factor. Then, from the study of a simplified linear solution of the eigenvalues of the non-uniformly accelerated system we

1. show that the classical MORFAC acceleration results from the acceleration of the mere sediment continuity equation;
2. obtain MASSPEED, a new linear morphodynamic acceleration technique, in which both mass continuity equations for water and sediment are accelerated by the same quantity;
3. set the basis for the derivation of a criterion for the a priori determination of the highest acceleration factor. It turned out that the MASSPEED can be successfully applied on a wider range of flow and sediment transport conditions as compared with the classical MORFAC approach;

Building on the knowledge obtained from the linear analysis, we derived a practical and implementable criterion for the determination of the maximum acceleration factor for both techniques. The accuracy of

the numerical solution can be determined by the user through the choice of a small tolerance value. This quantifies the extension of the range of validity under which the bed level can be linearly accelerated. The new criterion was implemented within an existing code following an adaptive concept in a similar manner as the CFL stability condition. Thanks to this adaptive procedure, the maximum accelerating factor is chosen at each time step according to the actual flow and sediment transport conditions. The numerical solution of the long term evolution of a sediment hump demonstrated that the application of the MASSPEED approach results in larger speed-up and considerable reduction of the computational time. It is also worth remarking the most important limitations of the proposed approach. The results presented are based on a few, strategic model simulations of the simple case of the one-dimensional propagation of a sediment hump under almost constant flow conditions. Therefore, they must be cautiously used when non-uniform morphology and time varying nonlinear forcing which may include tides, flood waves, etc. comes to modelling. It is likely that, in these cases, the maximum acceleration factor must be considerably decreased. In particular, we found that the higher the Fr is, the smaller will be the acceleration; furthermore, it is likely that the more unsteady the flow is, the smaller will be the possible acceleration. Bearing in mind these limitations, the theoretical background presented in this provides a robust basis for further exploring new morphological accelerators and extending the limit of applicability of the MASSPEED approach. Moreover, following a similar approach, the application of the MASSPEED approach can be extended to future trends, including: unsteady flow conditions, 2D (planar) morphological models, suspended transport and the de Saint Venant-Exner-Hirano model for non-uniform sediment deposition.

Acknowledgements

Part of this work has been carried out during Francesco Carraro’s visit to the Laboratory of Hydrology, Hydraulics and Glaciology of the Swiss Federal Institute of Technology. His staying was partially supported by the University of Ferrara through the 5% fees donation within the “Young Researcher Project”. Valerio Caleffi’s research has been funded by the University of Ferrara within the Founding Program FIR 2016, project title “Energy-preserving numerical models for the Shallow Water Equations”. We are also grateful to Prof. K. Hutter for reading the first draft of the manuscript.

Appendix A. Analytical study of the the bottom evolution

For $Fr \ll 1$ and $\psi \ll 1$, the governing system (1) is well approximated by the *decoupled form* (13). From a mathematical point of view, Eq. (13) implies that the decoupling is possible when the conservative variable z coincides with one of the three characteristic variables of the morphodynamic problem. A worthy example to better understand this feature is the linearised problem proposed in [18] and considered in §6.1.

To verify the validity of the decoupled formulation, the contribution of each eigenvalue (and the corresponding eigenvector) to the bed evolution is analysed, both in terms of bed forms celerity and amplitude.

The prototype problem [18] is governed by the *linearized original system* of Eqs. (44)-(45) (here reproduced for readability),

$$\frac{\partial \mathbf{W}}{\partial t} + \mathcal{A}_L \frac{\partial \mathbf{W}}{\partial x} = 0 \quad \text{with:} \quad \mathcal{A}_L = \mathcal{A}(\mathbf{W}_L) = \begin{bmatrix} 0 & 1 & 0 \\ c_L^2 - u_L^2 & 2u_L & c_L^2 \\ -u_L \psi_L & \psi_L & 0 \end{bmatrix}, \quad (\text{A.1})$$

where subscript L refers to the unperturbed state used to linearise the problem. Therefore, given the vector of unperturbed conservative variables $\mathbf{W}_L = [h_L, q_L, z_L]^T$, $u_L = q_L/h_L$ is the flow velocity; $c_L = \sqrt{g h_L}$ is the unperturbed celerity; while ψ_L is the uniform sediment transport as defined in (6).

The initial condition of the problem is given by

$$\mathbf{W}_0(x) = \begin{bmatrix} h_L \\ q_L \\ z_0 \end{bmatrix}, \quad (\text{A.2})$$

where: $z_0(x) = z_{\max} \exp(-x^2)$ with $z_{\max} = 1.0^{-5}$ m, $h_L = 1$ m, $q_L = \sqrt{h_L^3 g \text{Fr}_L^2}$, $\text{Fr}_L = 0.7$ and $\psi_L = 0.01$. Finally, a propagation time $t_p = 15$ s is assumed.

The linearized system (A.1) can be analytically solved by adopting the characteristic method [28] and using the analytical eigenvalues and eigenvectors of Appendix B (with $M_{cw} = M_q = M_{cs} = 1$). Thus, the conservative variables $\mathbf{W}(x)$ can be projected on the characteristic space multiplying them by the inverse of the matrix of the right eigenvectors of \mathcal{A}_L ,

$$\mathbf{U}(x) = \mathbf{L}_L \mathbf{W}(x), \quad (\text{A.3})$$

with $\mathbf{U}(x)$ the vector of the characteristic variables and $\mathbf{L}_L = \mathbf{R}_L^{-1}$ the inverse of the matrix of the right eigenvectors computed for the unperturbed state. Therefore, the initial conditions in terms of characteristic variables are $\mathbf{U}_0(x) = \mathbf{L}_L \mathbf{W}_0(x)$.

Each characteristic variable $\mathbf{U}^{(j)}$ satisfy a linear advection equation with a celerity given by the corresponding constant eigenvalue, λ_j^L , of \mathcal{A}_L , i.e.,

$$\frac{\partial \mathbf{U}^{(j)}}{\partial t} + \lambda_j^L \frac{\partial \mathbf{U}^{(j)}}{\partial x} = 0 \quad \text{for } j = 1, 2, 3. \quad (\text{A.4})$$

The corresponding solution in terms of \mathbf{U} , for a given x and t is

$$\mathbf{U}^{(j)}(x, t) = \mathbf{U}_0^{(j)}(x - \lambda_j^L t) \quad \text{for } j = 1, 2, 3. \quad (\text{A.5})$$

The evolved conservative variables $\mathbf{W}(x, t)$ can be found by multiplying $\mathbf{U}(x, t)$ by the matrix of the right eigenvectors \mathbf{R}_L ,

$$\mathbf{W}(x, t) = \mathbf{R}_L \mathbf{U}(x, t). \quad (\text{A.6})$$

Focusing the attention on the bottom evolution, and indicating with $\mathbf{r}_j^{(3)}$ the third component of the j -th eigenvector of \mathcal{A}_L , the third equation of the system (A.6) can be written as

$$z(x, t) = \sum_{j=1}^3 \mathbf{r}_j^{(3)} \mathbf{U}^{(j)}(x, t) = \sum_{j=1}^3 \zeta_j(x, t), \quad (\text{A.7})$$

where $\zeta_j(x, t) = \mathbf{r}_j^{(3)} \mathbf{U}^{(j)}(x, t)$ represents the contribution of each component of the characteristic variables to the bottom evolution.

Numbering the eigenvalues as defined in §2.3 and computing the eigenvectors as in Eq. (B.6), Fig. A.12a shows the comparison of the three terms $\zeta_j(x, t)$. The figure shows that the only meaningful contribution to the bed evolution is given by $\zeta_3(x, t) = \mathbf{r}_3^{(3)} \mathbf{U}^{(3)}(x, t)$ that implies $\zeta_3(x, t) \approx z(x, t)$. Furthermore, because the time evolution of $\mathbf{U}^{(3)}(x, t)$ is governed by the linear advection equation (A.5), the bed form migration celerity is $\lambda_3^L = \lambda_b$, as stated by Eq. (12).

Applying again the characteristic method [28] to the linearized MORFAC and MASSPEED systems (see, (45) of §6.1), accelerated dSVE problems can be solved. According to (A.5) and (A.7), the bottom evolution is properly accelerated if the characteristic variable $\zeta_3 \approx z$ is not altered by the acceleration, while the corresponding eigenvalues λ_3^L increase proportionally to the acceleration itself. For example, if accelerations of MF and MS are applied, the bed evolution is well represented if, at the *scaled propagation times* $t_p^{\text{MF}} = t_p/\text{MF}$ and $t_p^{\text{MS}} = t_p/\text{MS}$, the accelerated bottom elevations can be expressed as

$$\zeta_3^{\text{MF}}(x, t_p^{\text{MF}}) \approx \zeta_3^{\text{MS}}(x, t_p^{\text{MS}}) \approx \zeta_3(x, t_p) \approx z(x, t_p), \quad (\text{A.8})$$

with the accelerated eigenvalues

$$\frac{\lambda_3^{\text{MF}}}{\text{MF}} \approx \frac{\lambda_3^{\text{MS}}}{\text{MS}} \approx \lambda_3^L. \quad (\text{A.9})$$

For this linearised example with $\text{MF} = \text{MS} = 5$ and $t_p^{\text{MF}} = t_p^{\text{MS}} = 3$ s, Eq. (A.8) is verified, as shown in Fig. A.12b (MORFAC system) and Fig. A.12c (MASSPEED system). Indeed, according to Eq. (A.3) and (A.7), the evolved bottom function is related to both $\mathbf{r}_3^{(3)}$ and $\mathbf{l}_3^{(3)}$, so that any acceleration strategy must not alter these two quantities. The component $\mathbf{r}_3^{(3)}$ of the three linear systems, from Eqs. (6) and (B.6) can be written as

$$\mathbf{r}_3^{(3)} = \psi \frac{M_{\text{cs}}}{M_{\text{cw}}} \left(1 - \frac{u M_{\text{cw}}}{\lambda_3} \right), \quad (\text{A.10})$$

which becomes

$$\mathbf{r}_3^{(3)}|_{\text{OS}} = \psi \left(1 - \frac{u}{\lambda_3^L} \right), \quad \text{for the original system,} \quad (\text{A.11})$$

$$\mathbf{r}_3^{(3)}|_{\text{MF}} = \psi \text{MF} \left(1 - \frac{u}{\lambda_3^{\text{MF}}} \right), \quad \text{for the MORFAC system,} \quad (\text{A.12})$$

$$\mathbf{r}_3^{(3)}|_{\text{MS}} = \psi \left(1 - \frac{u \text{MS}}{\lambda_3^{\text{MS}}} \right), \quad \text{for the MASSPEED system.} \quad (\text{A.13})$$

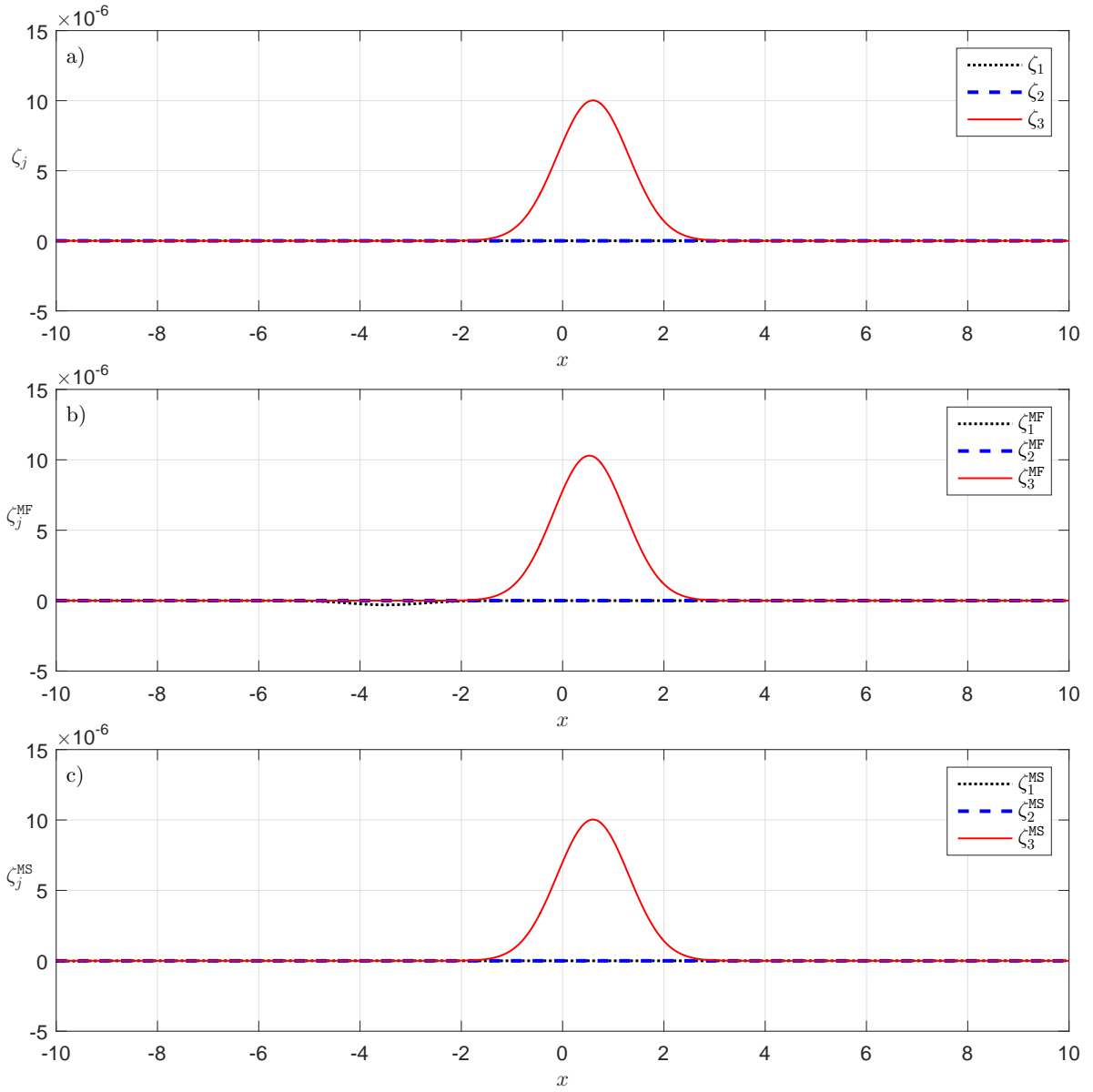


Figure A.12: The contributions of the three characteristic variables ζ_j to the bottom topography ($\text{Fr}_L = 0.7$; $\psi_L = 0.01$). a) solution of the linearized original system at t_p ; b) ζ_j^{MF} solution of the linearized MORFAC system with $\text{MF} = 5$ at t_p/MF ; c) ζ_j^{MS} solution of the linearized MASSPEED system with $\text{MS} = 5$ at t_p/MS .

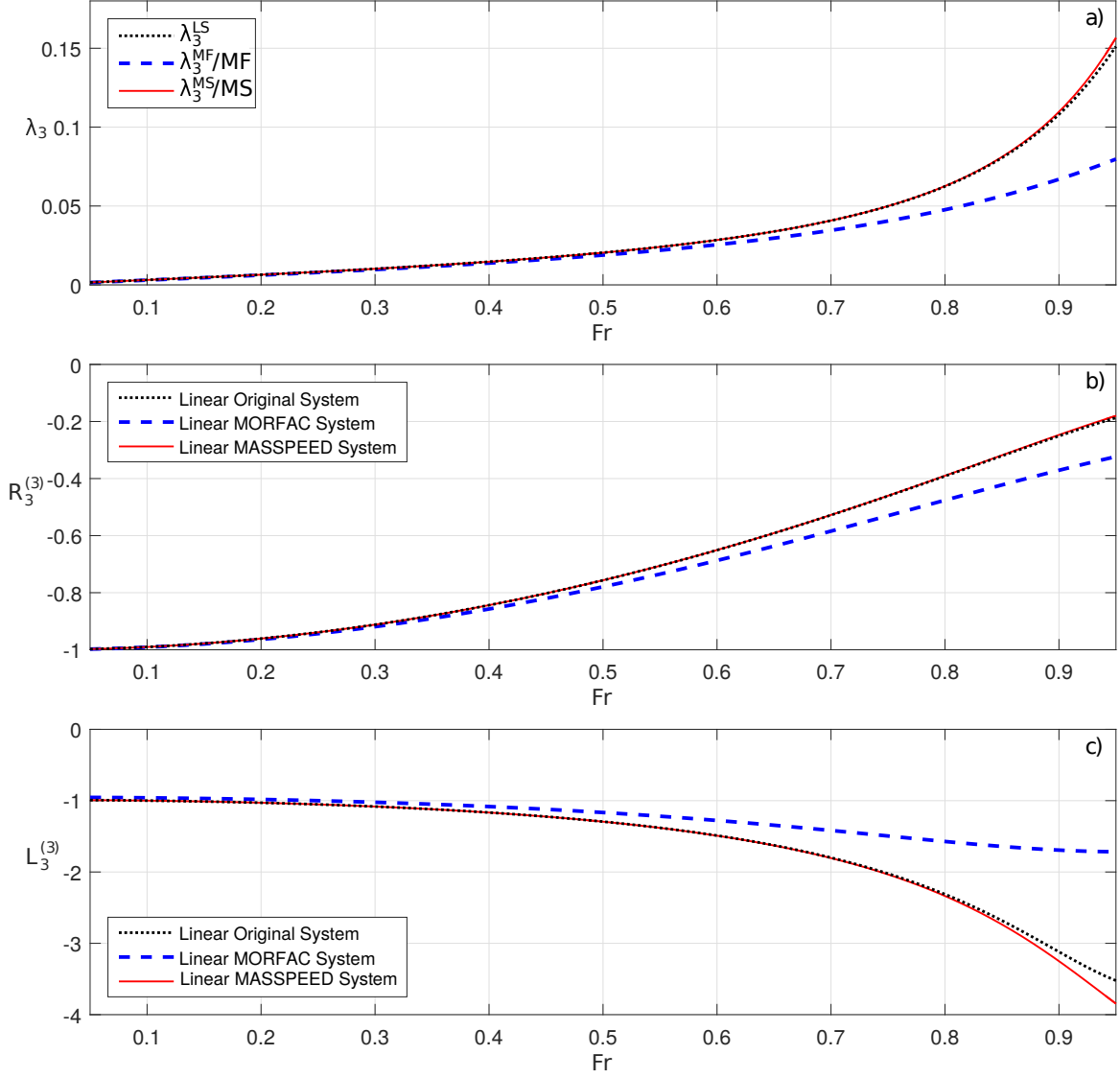


Figure A.13: Comparison between eigenstructure components for $0 < Fr_L < 0.95$, $\psi_L = 0.01$ and $MF = MS = 5$: a) acceleration of the third eigenvalue according to Eq. (A.9); b) $r_3^{(3)}$ according to the linearised original system, the linearised MORFAC system and the linearised MASSPEED system; c) $l_3^{(3)}$ according to the linearised original system, the linearised MORFAC system and the linearised MASSPEED system.

For the MASSPEED approach, looking at Eqs. (A.11) and (A.13), it is trivial to see that, if condition (A.9) is verified and then $\mathbf{r}_3^{(3)}|_{\text{MS}} \approx \mathbf{r}_3^{(3)}|_{\text{OS}}$, the acceleration technique does not alter the amplitude of the bed form. Conversely, for the MORFAC approach, looking at Eqs. (A.11) and (A.12), condition (A.9) is necessary but not sufficient to have $\mathbf{r}_3^{(3)}|_{\text{MF}} \approx \mathbf{r}_3^{(3)}|_{\text{OS}}$. Due to the lack of acceleration of the hydrodynamic continuity equation, MORFAC approximate $\mathbf{r}_3^{(3)}$ well only if $\text{MF} \approx 1$.

We can conclude that an exact linear scaling of the third eigenvalue is crucial to reproduce the propagation time of a bottom hump well, but also to preserve the correct profile of the riverbed. As discussed in §4, the MASSPEED extends the range of linear scaling of $\lambda_3^{\text{MS}}/\text{MS}$ with respect to $\lambda_3^{\text{MF}}/\text{MF}$ of the MORFAC approach.

This general result is confirmed also by Fig. A.13: it shows, for $0 < \text{Fr}_L < 0.95$, the comparison between the third eigenvalue and the corresponding component of \mathbf{R} and \mathbf{L} . According to Fig. A.13a, assuming as reference the original system, the MASSPEED gives a better approximation of the third eigenvalue, specially for $\text{Fr} > 0.6$ (for a more extended analysis of the effects of the parameter changes on the λ_3 eigenvalue, see §5). As a consequence, with respect to the classical MORFAC approach, the MASSPEED leads also to a much better approximation of $\mathbf{r}_3^{(3)}$ (Fig. A.13b) and $\mathbf{l}_3^{(3)}$ (Fig. A.13c). Thus, the improvement obtained by using the MASSPEED approach with respect to the MORFAC approach is clear.

Appendix B. Analytical eigenvalues and eigenvectors of the general governing system

The analysis presented in this work is based on the eigenvalues and eigenvectors of different governing systems, e.g. the original system, Eq. (4), or the accelerated system, Eq. (15). Therefore, the analytical closed expressions of the eigenvalues and eigenvectors are useful.

In this appendix we give the explicit formulations of such eigenvalues and eigenvectors for the following very general system:

$$\frac{\partial \mathbf{W}}{\partial t} + \mathcal{M} \mathcal{A} \frac{\partial \mathbf{W}}{\partial x} = 0, \quad (\text{B.1})$$

where

$$\mathbf{W} = \begin{bmatrix} h \\ q \\ z \end{bmatrix}, \quad \mathcal{A}(\mathbf{W}) = \begin{bmatrix} 0 & 1 & 0 \\ c^2 - u^2 & 2u & c^2 \\ \xi \frac{\partial q_s}{\partial h} & \xi \frac{\partial q_s}{\partial q} & 0 \end{bmatrix}, \quad \mathcal{M} = \begin{bmatrix} \text{M}_{\text{cw}} & 0 & 0 \\ 0 & \text{M}_{\text{q}} & 0 \\ 0 & 0 & \text{M}_{\text{cs}} \end{bmatrix}. \quad (\text{B.2})$$

The characteristic polynomial of the system is obtained by evaluating $|\mathcal{M} \mathcal{A}(\mathbf{W}) - \lambda \mathbf{I}| = 0$, i.e..

$$\lambda^3 - 2\text{M}_{\text{q}} u \lambda^2 + \text{M}_{\text{q}} \left(\text{M}_{\text{cw}} \text{Fr}^2 - \text{M}_{\text{q}} - \text{M}_{\text{cs}} \xi \frac{\partial q_s}{\partial q} \right) \frac{u^2}{\text{Fr}^2} \lambda - \text{M}_{\text{cs}} \text{M}_{\text{cw}} \text{M}_{\text{q}} \frac{u^2}{\text{Fr}^2} \xi \frac{\partial q_s}{\partial h} = 0, \quad (\text{B.3})$$

and the analytical solutions of the characteristic polynomial (B.3) can be computed by using the Cardano

formulas [1] leading to

$$\begin{aligned}\frac{\lambda_1}{c} &= \frac{2}{3}M_q \mathbf{Fr} - \frac{2}{3}\sqrt{k_2} \cos\left(\frac{\phi}{3} - \frac{\pi}{3}\right), \\ \frac{\lambda_2}{c} &= \frac{2}{3}M_q \mathbf{Fr} + \frac{2}{3}\sqrt{k_2} \cos\left(\frac{\phi}{3}\right), \\ \frac{\lambda_3}{c} &= \frac{2}{3}M_q \mathbf{Fr} - \frac{2}{3}\sqrt{k_2} \cos\left(\frac{\phi}{3} + \frac{\pi}{3}\right),\end{aligned}\tag{B.4}$$

where:

$$\begin{aligned}\phi &= \arccos\left(\frac{k_1}{\sqrt{4k_2^3}}\right), \\ k_1 &= 2M_q^2 \mathbf{Fr} \left(8M_q \mathbf{Fr}^2 + 9M_{cs} \xi \frac{\partial q_s}{\partial q} + 9M_{cw} (1 - \mathbf{Fr}^2)\right) + 27M_{cw} M_q M_{cs} \xi \frac{\partial q_s}{\partial h}, \\ k_2 &= 4M_q^2 \mathbf{Fr}^2 + 3M_q M_{cs} \xi \frac{\partial q_s}{\partial q} + 3M_{cw} M_q (1 - \mathbf{Fr}^2).\end{aligned}\tag{B.5}$$

Given the eigenvalue λ_i , the associated right eigenvector \mathbf{r}_i can be computed by solving the linear system $\mathcal{M}\mathbf{A}\mathbf{r}_i = \lambda_i \mathbf{r}_i$. Therefore, the matrix \mathbf{R} of the right eigenvectors can be expressed as a function of the eigenvalues, the result being

$$\mathbf{R} = [\mathbf{r}_1, \mathbf{r}_2, \mathbf{r}_3], \quad \text{with: } \mathbf{r}_i = \left[1, \frac{\lambda_i}{M_{cw}}, \xi \frac{M_{cs}}{M_{cw}} \left(\frac{M_{cw}}{\lambda_i} \frac{\partial q_s}{\partial h} + \frac{\partial q_s}{\partial q}\right)\right]^T.\tag{B.6}$$

For a given sediment transport formula that allows evaluating the q_s derivatives, eigenvalues and eigenvectors can be computed by substituting in Eqs. (B.4), (B.5) and (B.6), respectively: ($M_{cw} = M_q = M_{cs} = 1$) for the original system; ($M_{cw} = M_q = 1$, $M_{cs} = MF$) for the MORFAC system; and ($M_q = 1$, $M_{cw} = M_{cs} = MS$) for the MASSPEED system.

References

- [1] Birkhoff, G., Mac Lane, S., 1996. A Survey of Modern Algebra, 5th ed. New York: Macmillan.
- [2] Carraro, F., Caleffi, V., Valiani, A., 2016. Comparison between different methods to compute the numerical fluctuations in path-conservative schemes for SWE-Exner model. In: Erpicum, S., Dewals, B., Archambeau, P., Piroton, M. (Eds.), Sustainable Hydraulics in the Era of Global Change: Proceedings of the 4th IAHR Europe Congress. Taylor & Francis Group, Liege Belgium, pp. 699–706.
URL <http://www.crcnetbase.com/doi/pdfplus/10.1201/b21902-118>
- [3] Carraro, F., Caleffi, V., Valiani, A., 2017. Efficiency optimization of the DOT Riemann solver for Saint-Venant-Exner morphodynamic model. Submitted.
- [4] Coco, G., Zhou, Z., Van Maanen, B., Olabarrieta, M., Tinoco, R., Townend, I., 2013. Morphodynamics of tidal networks: advances and challenges. Marine Geology 346, 1–16.
- [5] Cordier, S., Le, M. H., Morales de Luna, T., 2011. Bedload transport in shallow water models: Why splitting (may) fail, how hyperbolicity (can) help. Advances in Water Resources 34 (8), 980–989.
- [6] De Vriend, H., Capobianco, M., Chesher, T., De Swart, H. d., Latteux, B., Stive, M., 1993. Approaches to long-term modelling of coastal morphology: a review. Coastal Engineering 21 (1-3), 225–269.
- [7] De Vries, M. (Ed.), 1965. Considerations about non-steady bed-load transport in open channels. No. 3.8.1-3.8.8 in Int. Assn. Hydraulic Research. Leningrad.

- [8] Dumbser, M., Toro, E. F., 2011. A Simple Extension of the Osher Riemann Solver to Non-conservative Hyperbolic Systems. *Journal of Scientific Computing* 48 (1-3), 70–88.
URL <http://link.springer.com/10.1007/s10915-010-9400-3>
- [9] Duró, G., Crosato, A., Tassi, P., 2016. Numerical study on river bar response to spatial variations of channel width. *Advances in Water Resources* 93, 21–38.
- [10] Grass, A. J., 1981. Sediment transport by waves and currents. University College, London, Dept. of Civil Engineering.
- [11] Isaacson, E., Temple, B., 1992. Nonlinear resonance in systems of conservation laws. *SIAM Journal on Applied Mathematics* 52 (5), 1260–1278.
- [12] Lanzoni, S., Siviglia, A., Seminara, G., 2006. Long waves in erodible channels and morphodynamic influence. *Water Resources Research* 42, w06D17, doi:10.1029/2006WR004916.
- [13] Latteux, B., 1995. Techniques for long-term morphological simulation under tidal action. *Marine Geology* 126 (1-4), 129–141.
- [14] Lesser, G. R., Roelvink, J. A., van Kester, J. A. T. M., Stelling, G. S., 2004. Development and validation of a three-dimensional morphological model. *Coastal Engineering* 51 (8-9), 883–915.
URL <http://linkinghub.elsevier.com/retrieve/pii/S0378383904000870>
- [15] Li, L., 2010. A fundamental study of the morphological acceleration factor. Ph.D. thesis, Delft University of Technology.
URL <https://repository.tudelft.nl/islandora/object/uuid:2780f537-402b-427a-9147-b8652279a83e?collection=education>
- [16] Liu, T.-P., 1987. Nonlinear resonance for quasilinear hyperbolic equation. *Journal of mathematical physics* 28 (11), 2593–2602.
- [17] Lyn, D., 1987. Unsteady sediment transport modeling. *Journal of Hydraulic Engineering* 113 (1), 1–15.
- [18] Lyn, D. a., Altinakar, M., 2002. St. Venant–Exner Equations for Near-Critical and Transcritical Flows. *Journal of Hydraulic Engineering* 128 (6), 579–587.
- [19] Meyer-Peter, E., Müller, R., 1948. Formulas for Bed-Load Transport. *Proceedings of the 2nd Meeting of the International Association of Hydraulic Research*, 39–64.
- [20] Mosselman, E., Le, T. B., 2016. Five common mistakes in fluvial morphodynamic modeling. *Advances in Water Resources* 93 (Part A), 15–20.
- [21] Nicholas, A. P., 2013. Modelling the continuum of river channel patterns. *Earth Surface Processes and Landforms* 38 (10), 1187–1196.
- [22] Oorschot, M. v., Kleinhans, M., Geerling, G., Middelkoop, H., 2015. Distinct patterns of interaction between vegetation and morphodynamics. *Earth Surface Processes and Landforms*.
- [23] Ranasinghe, R., Swinkels, C., Luijendijk, A., Roelvink, D., Bosboom, J., Stive, M., Walstra, D., 2011. Morphodynamic upscaling with the MORFAC approach: Dependencies and sensitivities. *Coastal Engineering* 58 (8), 806–811.
URL <http://dx.doi.org/10.1016/j.coastaleng.2011.03.010>
- [24] Roelvink, J., 2006. Coastal morphodynamic evolution techniques. *Coastal Engineering* 53 (2-3), 277–287.
URL <http://linkinghub.elsevier.com/retrieve/pii/S0378383905001419>
- [25] Roelvink, J. D., Walstra, D.-J. R., van der Wegen, M., Ranasinghe, R., 2016. Modeling of coastal morphological processes. In: Dhanak, M. R., Xiros, N. I. (Eds.), *Springer Handbook of Ocean Engineering*. Springer International Publishing, Cham, Ch. 28, pp. 611–634.
URL http://dx.doi.org/10.1007/978-3-319-16649-0_28
- [26] Siviglia, A., Crosato, A., 2016. Numerical modelling of river morphodynamics: Latest developments and remaining challenges. *Advances in Water Resources* 93 (Part A), 1–3.
- [27] Siviglia, A., Stecca, G., Vanzo, D., Zolezzi, G., Toro, E. F., Tubino, M., 2013. Numerical modelling of two-dimensional

- morphodynamics with applications to river bars and bifurcations. *Advances in Water Resources* 52, 243–260.
- [28] Toro, E., 2009. *Riemann Solvers and Numerical Methods for Fluid Dynamics*, 3rd Edition. Springer US.
- [29] Traub, J., 1982. *Iterative Methods for the Solution of Equations*. AMS Chelsea Publishing Series. Chelsea.
URL <https://books.google.it/books?id=se3YdgFgz4YC>